Cognitive Beamforming Transmission and Energy Harvesting with Limited Primary Cooperation: Analysis and Design

by

Tianqing Wu
B.Eng., Beijing University of Posts and Telecommunications, Beijing, China, 2007
M.Eng., Beijing University of Posts and Telecommunications, Beijing, China, 2010

A Dissertation Submitted in Partial Fulfillment of the
Requirements for the Degree of

DOCTOR OF PHILOSOPHY

in the Department of Electrical and Computer Engineering

Cognitive Beamforming Transmission and Energy Harvesting with Limited Primary Cooperation: Analysis and Design

by

Tianqing Wu
B.Eng., Beijing University of Posts and Telecommunications, Beijing, China, 2007
M.Eng., Beijing University of Posts and Telecommunications, Beijing, China, 2010

Supervisory Committee

Dr. Hong-Chuan Yang, Supervisor
(Department of Electrical and Computer Engineering)

Dr. Daler N. Rakhmatov, Departmental Member
(Department of Electrical and Computer Engineering)

Dr. Kui Wu, Outside Member
(Department of Computer Science)

Supervisory Committee

Dr. Hong-Chuan Yang, Supervisor
(Department of Electrical and Computer Engineering)

Dr. Daler N. Rakhmatov, Departmental Member
(Department of Electrical and Computer Engineering)

Dr. Kui Wu, Outside Member
(Department of Computer Science)

ABSTRACT

Cognitive radio improves radio spectrum utilization either by spectrum sharing or by opportunistically utilizing the spectrum of the licensed users. Cognitive beamforming is a prominent technique that can further enhance the overall performance of the wireless communication systems through beamforming vector design and/or power allocation. Harvesting radio frequency (RF) energy from existing wireless communication systems is a promising potential solution for providing convenient, perpetual and green energy supply to wireless sensor networks (WSN). The amount of energy that can be harvested from existing RF energy sources over a short period of time can only support low data rate applications with simply transmission strategies. The main challenge for satisfying the energy requirement of WSN is the time-varying wireless fading channels. Low complexity cooperation between WSN and RF energy source can effectively enhance the stability of energy supply for the sensor node. While multiple transmission antennas are deployed at the existing RF energy source, judicious transmit beam selection can further improve the harvested energy at the sensor node, while simultaneously serving multiple users.

In this doctoral research, we present random unitary beamforming (RUB) cooperative beam selection schemes to ensure the QoS of primary system and reduce the

hardware and software complexities of secondary system. We analyze the exact outage performance of the primary system, and investigate the tradeoff between primary system outage probability versus secondary system sum-rate performance. We also study the performance of overlaid wireless sensor transmission powered by RF energy harvested from existing wireless system. We derive the exact distribution function of harvested energy over a certain number channel coherence time over Rayleigh fading channels with the consideration of hardware limitation, such as energy harvesting sensitivity and harvesting efficiency. We also analyze the average packet delay and packet loss probability of sensor transmission subject to interference from existing system, for both delay insensitive traffics and delay sensitive traffics. The optimal design of energy storage capacity of the sensor nodes is proposed to minimize the average packet transmission delay for delay insensitive traffics with two candidate transmission strategies. We further investigate the energy harvesting performance of a wireless sensor node powered by RF energy from an existing multiuser MIMO system. Specifically, we propose based cooperative beam selection schemes to enhance the energy harvesting performance at the sensor. We derive the exact distribution function of harvested energy in a coherence time and further investigate the performance tradeoff of the average harvested energy at the sensor versus the sum-rate of the multiuser MIMO system.

Contents

List of Figures

ACKNOWLEDGEMENTS

I would like to take this opportunity to thank all those who contributed to the success of this work. I am very thankful to my supervisor, Dr. Hong-Chuan Yang, for supporting me both financially and academically during my graduate studies. He has been a constant source of knowledge, inspiration and encouragement for me.

I am also deeply grateful to Dr. Daler N. Rakhmatov for serving as the department member, Dr. Kui Wu and Dr. Yindi Jing as the outside member in my supervisory committee. Their comments and suggestions have greatly improved my dissertation. I am also appreciative of Dr. Ying-Chang Liang for his time and valuable comments on the proposed schemes for cooperative MIMO systems in Chapter 2. Finally, I am also appreciative of Dr. Peng Lu who contributed to an algorithm that I used to develop some of the simulation results given in Chapter 2 and Chapter 4.

Chapter 1

Introduction

Wireless sensors are used in a wide range of applications, such as environment monitoring, surveillance, health care, intelligent buildings and battle field control [1]. The sensor nodes are usually powered by batteries with finite capacity, which manifests as an important limiting factor to the functionality of wireless sensor network (WSN). Replacing or charging the batteries may either incur high costs for human labor or be impractical for certain application scenarios (e.g. applications that require sensors to be embedded into structures). Powering sensor nodes through ambient energy harvesting has therefore received a lot of attentions in both academia and industrial communities [2, 3]. On the other hand, cognitive radio was proposed to solve the spectrum scarcity problem through spectrum sharing [38]. New wireless system can utilize the spectrum as long as its transmission will not create serious interference. Cognitive beamforming is a promising technique that enables a multi-antenna secondary transmitter to regulate its interference to primary system. Radio frequency (RF) energy harvesting and cognitive beamforming have emerged as two prominent techniques to obtain energy from and limit interference to currently deployed wireless communication systems, respectively. Below is a brief description of these two key enabling technologies of the next generation communication systems.

1.1 Cognitive Beamforming

Cognitive radio was first proposed in [38] to solve the spectrum scarcity problem through spectrum sharing. By allowing the secondary users (SUs) to access the spectrum allocated to a primary network, the spectrum utilization can be effectively

improved and more wireless services can be supported [39].

Cognitive radio implementation can be classified broadly into two paradigms: interweave and underlay implementations [38]. In the interweave implementation (also referred to as opportunistic spectrum access), the cognitive user first tries to detect the availability of spectrum holes (unoccupied band) in the licensed band through spectrum sensing. The main challenging aspect of this mode of communication is the spectrum sensing by the cognitive users, which is not only very challenging but also consumes a lot of power. With underlay implementation strategy, the primary network and cognitive network can transmit simultaneously while ensuring the interference from the secondary transmitter to the primary user is at a tolerable level [40].

In an underlay cognitive setting, a fundamental challenge is to ensure the Quality-of-Service (QoS) of the primary system while improving the performance of the secondary system [41]. Cognitive beamforming is a promising technique that enables a multi-antenna secondary transmitter to regulate its interference to primary receivers (PR) through beamforming vector design and/or power allocation [42]. The optimal cognitive beamforming design is considered in [42, 43, 44, 45, 46] with full or partial channel state information feedback from the primary system to the secondary system. The beamforming vector design is considered in [42] and [43] using partial channel state information. [42] attempts to minimize the outage probability of the secondary user while meeting the rate requirement of the primary user. In [43], the secondary link gain is maximized under the constraint of the interference at the primary user. In [44], joint zero-forcing beamforming and power allocation is studied to maximize the throughput on the secondary network, while keeping the interferece to the primary users at a tolerable level. However, [44] assumes perfect channel state information at the secondary base station (SBS), which is impractical due to the tremendous amount of feedback required from PRs. [45] and [46] extend the design to partial channel state information scenario. Note that these work can not guarantee the quality of PR received signal as PR link quality was not taken into consideration. In [47], the authors propose joint optimization algorithms of the beamforming vector and power allocation for the SBS in order to maximize the rate for the SU while meeting the rate requirement for the PR. Most of these designs assume that the beamforming vectors and power can be optimally determined based on instantaneous channel information of SU channels, which typically require heavy feedback load from SU and/or high calculation complexity at SBS.

Random unitary beamforming (RUB) is a low-complexity multi-antenna transmission scheme that requires very low feedback load, and thus has attracted continuing research interest [33, 34]. The base station with RUB only needs partial channel state information, usually in terms of the signal-to-interference-plus-noise ratio (SINR) on several randomly generated beam directions. It has been shown in [33] that if each user just feeds back its best beam index and the corresponding SINR, RUB can achieve the same sum-rate scaling law as the optimal dirty paper coding (DPC) transmission scheme [34]. However, most of previous works on RUB assume conventional multiuser multiple-input multiple-output (MIMO) systems, and very limited work considered RUB transmission in a cognitive radio network environment. Chapter 2 contains a detailed discussion on the cooperative beam selection strategies in an underlay cognitive radio.

1.2 RF Energy Harvesting

Recently, there has been a growing interest in RF energy harvesting due to the intensive deployment of cellular/WiFi wireless systems in addition to traditional radio/TV broadcasting systems [8]. It has been experimentally proved that RF energy harvesting is feasible from the hardware implementation viewpoint. In [9], the authors developed prototypes for devices that communicate with each other using ambient RF signals from TV/cellular systems as the only power source. In [10], the authors present the experimental performance (e.g., charging time of the sensor and received signal power at the sink) of RF energy harvesting using PowerCast energy harvesters [11]. Although these previous works have proved a visible future for the wireless applications based on RF energy harvesting, most performance results are obtained through laboratory experiments. There is still a lack of effective theoretical models that can analytically predict the performance of WSNs powered by RF energy harvesting.

Researchers have proposed different solutions to harvest RF energy from existing wireless communication systems. The fundamental performance limits of simultaneous wireless information and energy transfer systems over point-to-point link were studied in [23, 24]. In [25], the authors consider a three-node MIMO wireless system, where one receiver harvests energy and another receiver decodes information from the signal transmitted by a common transmitter. A cognitive network that can harvest RF energy from the primary system is considered in [26]. The authors

propose an optimal mode selection policy for sensor nodes to decide whether to transmit information or to harvest RF energy based on Markov modelling. In [27], the authors investigate mode switching between information decoding and energy harvesting, based on the instantaneous signal channel and interference condition over a point-to-point link. In most of these works, it is generally assumed that the channel gain remains constant during the whole energy harvesting circle, including obtaining channel state information, making decision accordingly, and then harvesting energy and/or decoding information. It worths to point out that wireless fading channels are in general time varying with channel coherence time in the order of milliseconds. The harvested energy over one channel coherence time may not be sufficient for channel estimation alone, not to mention information transmission/decoding.

On another front, considerable research effort has been carried out on the packet transmission performance analysis and optimization for WSN powered by harvesting energy from conventional energy sources [12, 13, 14, 15, 16, 17, 18, 19, 20, 21]. The optimal packet scheduling policies in an energy harvesting communication systems were investigated over AWGN channels under the assumption of predictable energy arrival in [12] and [13]. Specifically, [12] targets at minimizing the packet delivery delay under data and energy arrival causality constraints and [13] also takes into account the finite energy storage capacity. In [14, 15, 16, 17, 18, 19], throughput maximization and packet delay minimization problems with energy harvesting constraints are studied for different channel environments. In [20], energy management policies that stabilize the data buffer have been proposed for single-user communication scenario by applying linear energy-rate approximations. In [21], medium access control (MAC) protocols for single-hop wireless sensor networks are designed and analyzed. A save-then-transmit protocol is proposed in [22] to minimize the outage probability of energy harvesting transmitters by finding the optimal time fraction for energy harvesting in a time slot, during which the wireless channel is assumed to be constant. It is worth noting that these works can not directly apply to RF energy harvesting. First of all, most of these work focus on the design of off-line packet scheduling strategies with predictable channel or energy state information, which is not available for RF energy harvesting over time-varying wireless channels. Furthermore, the amount of energy that can be harvested from RF energy sources over a short period of time (e.g. a channel coherence time) is typically much less than that from conventional energy sources. As such, WSN powered with RF energy harvesting can only support low data rate applications with simply transmission strategies.

In this dissertation, we propose several practical low-complexity RF energy harvesting schemes, where the wireless sensor harvests RF energy from multiple antennas and multiple channel coherence time over time-varying wireless channels. These solutions will be discussed in a greater detail in Chapter 3 and 4.

1.3 Dissertation Outline

The main focus of the dissertation is on the cognitive beamforming transmission with RF energy harvesting for the next generation cooperative wireless communication systems. Whenever feasible, we derive the exact analytical expression for the performance metrics of interest in simple closed form, which facilitates fast evaluation and convenient applications to parameter optimization. These analytical results will help determine what type of applications that the proposed overlaid implementation strategy can effectively support. The rest of the thesis is organized as follows.

Chapter 2 investigates the performance of RUB based cooperative beam selection schemes, where the secondary multiuser MIMO system can determine the usability of each beamforming vector to guarantee the SINR requirement at the primary system. We propose cooperative beam selection strategies for both single SU and multiple SUs transmission cases, and obtain the outage performance of the primary system and sum-rate of the secondary system for both cases.

We consider an overlaid sensor transmission scenario where a sensor-to-sink communication link operates in the coverage of an existing wireless system over the same frequency in Chapter 3, where the sensor needs to harvest RF energy from the transmission of existing wireless system. Due to practical hardware constraints, the sensor node can only harvest RF energy when its received signal power is larger than a certain sensitivity level [25]. As such, the existing system, being either cellular, WiFi or TV broadcasting systems, serves as the ambient source for sensor energy harvesting and as interference source during sensor transmission. We investigate the packet transmission performance of the sensor-to-sink link over Rayleigh fading wireless channels. Specifically, we first consider delay sensitive scenario, where the sensor needs to periodically transmit a new packet to the sink with hard delay constraint. We evaluate the packet loss probability assuming no retransmission is allowed. For delay insensitive traffic, where the sensing data must be delivered to the sink without error at the expense of a certain delay, we calculate the average delay of packet transmission over the link with harvested energy.

Chapter 4 investigates the performance of RUB based cooperative RF energy harvesting schemes, where an existing multiuser MIMO system helps the energy harvesting of a RF-energy-powered sensor node, while simultaneously serving its own users. The existing multiuser MIMO system needs to select the best beams for transmission, while trying to satisfy energy harvesting requirement of the sensor. To evaluate the performance tradeoff between the average harvested energy at the sensor and the sum-rate of the existing multiuser MIMO system, we derive the closed-form statistical distribution of the amount of energy that can be harvested with the proposed cooperative RF energy harvesting scheme. These analytical results will help determine the optimal energy threshold value that can satisfy requirements of certain sensing applications, while considering the negative effect on the multiuser MIMO system.

Lastly, Chapter 5 provides the concluding remarks and points out some future research directions. All of the technical content presented in this dissertation is either already published in journal and conference papers. These papers are listed at the end of the dissertation before the references.

Chapter 2

Cooperative Secondary Beam Selection for Cognitive Multiuser MIMO Transmission with Random Beamforming

2.1 Introduction

In an underlay cognitive setting, a fundamental challenge is to ensure the QoS of the primary system while improving the performance of the secondary system [41]. Cognitive beamforming is a promising technique that enables a multi-antenna secondary transmitter to regulate its interference to primary receivers (PR) through beamforming vector design and/or power allocation [42]. The optimal cognitive beamforming design is considered in[42, 43, 44, 45, 46] with full or partial channel state information feedback from the primary system to the secondary system. Most of these designs assume that the beamforming vectors and power can be optimally determined based on instantaneous channel information of SU channels, which typically require heavy feedback load from SU and/or high calculation complexity at secondary base station (SBS).

Random unitary beamforming (RUB) is a low-complexity multi-antenna transmission scheme that requires very low feedback load, and thus has attracted continuing research interest [33, 34]. In this Chapter, we adopt RUB as the transmission scheme for the secondary multiuser MIMO system. To ensure the performance requirement

of the primary system, i.e. the received SINR at PR is larger than a predefined SINR threshold, the PR will feed back to the SBS its received signal power from primary transmitter (PT), such that the SBS can calculate the received SINR at PR and determine the usability of each beamforming vector. Such cooperation is required to guarantee the SINR requirement at PR. Note that PR may need to inform its received signal power to PT for rate adaptation purpose anyway. We propose cooperative beam selection strategies for both single SU and multiple SUs transmission cases. Specifically, for the single SU case, we propose a cooperative usable beam selection (CUBS) strategy, where the SBS calculates the received SINR at PR for each beam using the feedback from PR and channel estimation, and then determines those usable beams. The cooperation of PR in sending its received signal power is required to guarantee the received SINR at PR is acceptable.[1] The SBS then selects the best beam from all usable beams to serve it users. The SBS then selects the best beam from all usable beams to serve its user. Note that the SU only needs to feed back the index of the best usable beam to SBS. We derive the close form expression of the distribution of the number of the usable beams, based on which we obtain the exact throughput performance of the secondary system. We also derive the close-form upper bound for the outage probability of the primary system. Numerical examples show that the outage performance of the primary system will suffer burst degradation when the beam selection threshold is smaller than the outage threshold. This is because the secondary system may transmit with beams that lead to the received SINR at PR below the outage threshold. To avoid the burst increase of the outage probability of the primary system as well as achieve high secondary system throughput, the beam selection threshold should be equal to the outage threshold of the primary system.

For the multiple SUs case, the SBS needs to select a beam subset, such that the total interference with all beams in the subset active still lead to the received SINR at PR larger than the SINR threshold. We propose two cooperative beam selection strategies, termed as constant beam power cooperative active beam selection (CBP-CABS) strategy and constant total power cooperative active beam selection (CTP-CABS) strategy, depending on whether the transmission power on each beam

[1]With conventional underlay cognitive implementation, the SBS will design its transmission such that the received interference power at primary receiver is below a certain threshold. The received SINR at the primary receiver may be unsatisfactory if the received signal power from primary transmitter is low. Our proposed underlay approach guarantee the primary system quality while maximizing the transmission opportunities for the secondary systems.

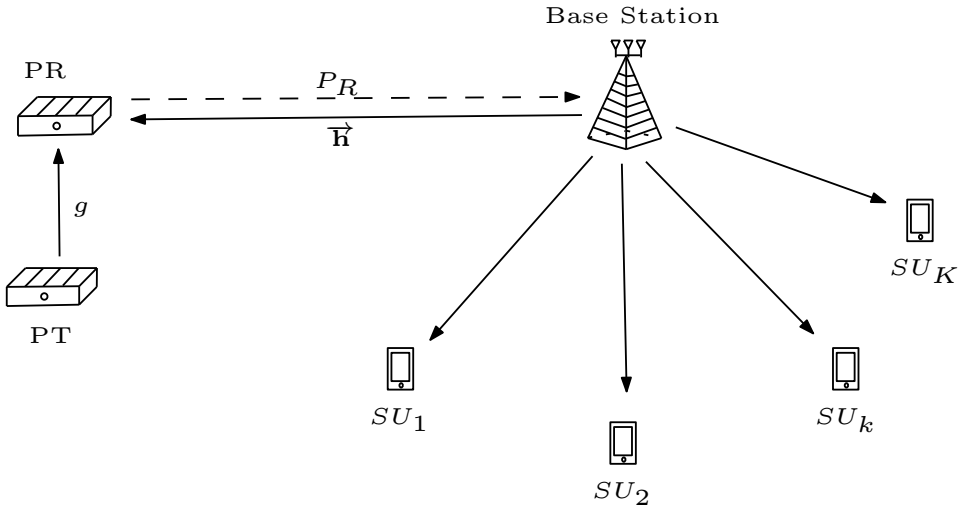

Figure 2.1: System and channel model.

changes with the number of active beams or not. For both strategies, SUs only need to feed back their received SINR on usable beam. To examine the performance tradeoff between the outage probability of the primary system and the sum-rate of the multiuser MIMO system for each strategy, we derive the closed-form expression of the outage probability of the primary system and sum-rate of the secondary system. Numerical examples show that CTP-CABS strategy can achieve larger sum-rate for the secondary system without significantly affecting the outage performance of the primary system.

The rest of this Chapter is organized as follows. In Section 2.2, the system and channel model for the primary system and secondary system is introduced. In Section 2.3, the cooperative beam selection strategy for single SU case is proposed, and we analyze the outage performance of the primary system and the throughput of the secondary system. Two cooperative beam strategies for multi-user case are presented in Section 2.4, together with performance trade-off analysis between primary and secondary system. Finally, we present some concluding remarks in Section 2.5.

2.2 System and Channel Model

We consider a RUB-based secondary multiuser MIMO system deployed in the coverage area of a primary system with single-antenna primary transmitter (PT) and primary receiver, as shown in Fig. 2.1. We assume the primary system operates

in a time-division duplexing (TDD) mode, over the channel frequency SUs want to access. The secondary system consists of single base station with M antennas and K single-antenna secondary users. The SBS can serve up to M SUs simultaneously using random orthonormal beams generated from an isotropic distribution. Let $\mathcal{W} = [\mathbf{w}_1, \mathbf{w}_2, \ldots, \mathbf{w}_M]^T$ denote the set of beam vectors, assumed to be known to both the SBS and its SUs. The transmitted signal vector from M antennas over one symbol period can be written as $\mathbf{x} = \sum_{j=1}^{M} \sqrt{P_j}\mathbf{w}_j s_j$, where s_j denotes the information symbol for the jth beam vector, and P_j denotes the transmission power allocated to the jth beam vector, which satisfies $\sum_{j=1}^{M} P_j \leq P_S$, where P_S denotes the maximum transmission power of the SBS.

We adopt a log-distance path loss plus slow Rayleigh fading channel models for the operating environment while ignoring the shadowing effect [30]. Let g denote the fading channel gain from PT to PR, where $g \in \mathcal{CN}(0, 1)$. The received signal power at PR can be given by

$$P_R = \frac{P_P}{\Gamma d_P^{\lambda}} |g|^2, \tag{2.1}$$

where P_P denotes the transmission power of PT, d_P denotes the distance from PT to PR, λ is the path loss exponent, ranging from 2 to 5, and Γ is a constant parameter of the log-distance model. Specifically, $\Gamma = \frac{PL(d_0)}{d_0^{\lambda}}$, where d_0 is a reference distance in the antenna far field, and $PL(d_0)$ is linear path loss at distance d_0, depending on the propagation environment.

Let $\mathbf{h} = [h_1, h_2, \ldots, h_M]^T$ denote the fading channel gain vector from the SBS to PR, where $h_m \in \mathcal{CN}(0, 1)$. The interference power at PR generated by the jth beam of the SBS transmission can be given by

$$I_j^{(P)} = \frac{P_j}{\Gamma d_I^{\lambda}} |\mathbf{h}^T \mathbf{w}_j|^2, \quad j = 1, 2, \ldots, M, \tag{2.2}$$

where d_I denotes the distance from SBS to PR. For notational conciseness, we use α_j to denote the amplitude square of the projection of $\mathbf{h}$ on to $\mathbf{w}_j$, i.e. $\alpha_j = |\mathbf{h}^T \mathbf{w}_j|^2$, whose probability density function (PDF) for Rayleigh fading channel under consideration is given by

$$f_{\alpha_j}(x) = e^{-x}. \tag{2.3}$$

In the followings, we propose simple and low-complexity cooperative beam selection (CBS) strategies for both single SU and multiple SUs cases.

2.3 Cooperative Usable Beam Selection for Single SU

For single SU case, the SBS uses a single active beam to serve its SU. We assume that the transmission power allocated to the active beam is P_S. To satisfy the QoS requirement of the primary system, i.e., the received SINR at PR is larger than a predefined SINR threshold γ_D, we propose a cooperative usable beam selection (CUBS) strategy to determine the usability of each beam.

2.3.1 Mode of Cooperation

At the beginning of each channel coherence time, PT sends a pilot signal to PR. PR estimates the received signal power P_R, and then sends it to the SBS. Based on the received signal from PR, SBS can obtain the channel gain vector $\mathbf{h}$ through channel estimation.[2] The SBS then calculates the received SINR at PR corresponding to each beam, given by

$$\gamma_m^{(P)} = \frac{P_R}{I_m^{(P)} + \sigma_P^2}, m = 1, 2, \ldots, M, \tag{2.4}$$

where $I_m^{(P)}$ is the interference at PR if mth beam is used, given by (2.2), σ_P^2 is the noise variance. The SBS compares $\gamma_m^{(P)}$ with γ_D for each beam. If $\gamma_m^{(P)} \geq \gamma_D$, the SBS adds the index m into a usable beam index set β. Then SU will feed back the index of the best usable beam by comparing the received power for each beam in set β. SBS will use the best beam that leads to the largest received signal power at SU for transmission.

With a certain synchronization mechanism, SBS can receive feedback information from PR and SUs correctly. Note that it may happen that $\gamma_m^{(P)}$ is smaller than γ_D for every beam. In this case, set β is empty. SBS will hold its transmission for a channel coherence time.

[2]Alternatively, the channel gain vector $\mathbf{h}$ can be estimated by the PR and fed back to the SBS, whereas the feedback load from PR to SBS increases with the size of $\mathbf{h}$.

2.3.2 Distribution of the Number of Usable Beams

In the following, we derive the probability mass function (PMF) of the number of beams M_a that the BS can use, which will be applied to the throughput analysis for the secondary system.

With the proposed cooperative beam selection scheme, the SBS will select the best beam to serve the user, while ensuring that the received SINR at PR is above a predefined SINR threshold γ_D. We denote the ordered version of the interference power caused by each beam to PR as $I_{1:M}^{(P)}, I_{2:M}^{(P)}, \ldots, I_{M:M}^{(P)}$, where $I_{1:M}^{(P)} \geq I_{2:M}^{(P)} \geq \cdots \geq I_{M:M}^{(P)}$. Then the ith largest received SINR at PR, denoted by $\gamma_{i:M}^{(P)}$, can be written as

$$\gamma_{i:M}^{(P)} = \frac{P_R}{I_{M-i+1:M}^{(P)} + \sigma_P^2}, \quad 1 \leq i \leq M. \tag{2.5}$$

If the ith $(0 < i < M)$ largest SINR $\gamma_{i:M}^{(P)}$ is larger than γ_D, whereas the $(i+1)$th smallest beam $\gamma_{i+1:M}^{(P)}$ is smaller than γ_D, then the number of usable beams is $M_a = i$. If the received SINR at PR is larger than the threshold for all beams, i.e. $\gamma_{M:M}^{(P)} > \gamma_D$, then the number of usable beams is $M_a = M$. If the received SINR at PR is smaller than γ_D even when the SBS uses the beam corresponding to $\gamma_{1:M}^{(P)}$, i.e. $\gamma_{1:M}^{(P)} < \gamma_D$, the SBS will stop transmission to avoid interference to PR.

Therefore, the probability that M_a beams are usable can be given by

$$\Pr[M_a = i] = \begin{cases} \Pr[\gamma_{1:M}^{(P)} < \gamma_D], & i = 0, \\ \Pr[\gamma_{i:M}^{(P)} > \gamma_D, \gamma_{i+1:M}^{(P)} < \gamma_D], & 0 < i < M, \\ \Pr[\gamma_{M:M}^{(P)} > \gamma_D], & i = M. \end{cases} \tag{2.6}$$

After substituting (2.1) and (2.5) into (2.6) and some manipulations, (2.6) can be rewritten as

$$\Pr[M_a = i] = \begin{cases} \int_0^\infty \int_0^{\frac{\gamma_D}{\overline{P}_R}(y+\sigma_P^2)} f_{|g|^2}(x)dx f_{I_{M:M}^{(P)}}(y)dy, & i = 0, \\ \int_0^\infty \int_0^z \int_{\frac{\gamma_D}{\overline{P}_R}(y+\sigma_P^2)}^{\frac{\gamma_D}{\overline{P}_R}(z+\sigma_P^2)} f_{|g|^2}(x)dx f_{I_{M-i:M}^{(P)}, I_{M-i+1:M}^{(P)}}(z,y)dydz, & 0 < i < M, \\ \int_0^\infty \int_{\frac{\gamma_D}{\overline{P}_R}(y+\sigma_P^2)}^\infty f_{|g|^2}(x)dx f_{I_{1:M}^{(P)}}(y)dy, & i = M, \end{cases} \tag{2.7}$$

where $\overline{P}_R = \frac{P_P}{\Gamma d_P^\lambda}$ denotes the average received power at PR for notational conciseness,

and the PDF of $|g|^2$, $I_{1:M}^{(P)}$, and $I_{M:M}^{(P)}$, and the joint PDF of $I_{i:M}^{(P)}$ and $I_{i+1:M}^{(P)}$, can be given by [29]

$$f_{|g|^2}(x) = e^{-x}, \tag{2.8}$$

$$f_{I_{1:M}^{(P)}}(x) = \frac{M}{\overline{I}_P} e^{-\frac{x}{\overline{I}_P}} (1 - e^{-\frac{x}{\overline{I}_P}})^{M-1}, \tag{2.9}$$

$$f_{I_{M:M}^{(P)}}(x) = \frac{M}{\overline{I}_P} e^{-\frac{Mx}{\overline{I}_P}}, \tag{2.10}$$

and

$$f_{I_{i:M}^{(P)}, I_{i+1:M}^{(P)}}(x, y) = \frac{M! e^{-\frac{ix+y}{\overline{I}_P}} (1 - e^{-\frac{y}{\overline{I}_P}})^{M-i-1}}{(M-i-1)!(i-1)! \overline{I}_P^2}, 0 < i < M, \tag{2.11}$$

respectively, where $\overline{I}_P = \frac{P_S}{\Gamma d_I^\lambda}$ denotes the average received interference at PR. By substituting (2.8), (2.9), (2.10), and (2.11) into (2.7) and carrying out integration, the close form expression of $\Pr[M_a = i]$ is calculated as

$$\Pr[M_a = i] \;=\; \begin{cases} 1 - \frac{e^{-\frac{\gamma_D \sigma_P^2}{\overline{P}_R}}}{1 + \frac{\Lambda \gamma_D}{M}} & i = 0, \\ \frac{M! e^{-\frac{\gamma_D \sigma_P^2}{\overline{P}_R}}}{(M-i-1)!(i-1)!} \frac{\Lambda \gamma_D}{(M-i)(M-i+\Lambda\gamma_D)} \sum_{n=0}^{i-1} (-1)^n \binom{i-1}{n} \frac{1}{\Lambda\gamma_D + n + 1 + M - i} & 0 < i < M, \\ M e^{-\frac{\gamma_D \sigma_P^2}{\overline{P}_R}} \sum_{n=0}^{M-1} (-1)^n \binom{M-1}{n} \frac{1}{\Lambda\gamma_D + n + 1} & i = M, \end{cases} \tag{2.12}$$

where Λ is a constant parameter equal to $\frac{\overline{I}_P}{\overline{P}_R}$ for notational conciseness.

2.3.3 Throughput of the Secondary System

We are interested in the average throughput of the secondary system, which can be calculated as[3]

$$R = \sum_{i=1}^{M} \Pr[M_a = i] R_i, \tag{2.13}$$

where $\Pr[M_a = i]$ denotes the probability that i beams are usable for transmission, given in (2.12), and R_i denotes the average throughput when i beams are usable, which can be calculated as

$$R_i = \int_0^{\infty} \log_2(1+x) f_{\gamma_{1:i}^{(S)}}(x) dx, \quad i = 1, 2, \ldots, M, \tag{2.14}$$

where $f_{\gamma_{1:i}^{(S)}}(x)$ denotes the PDF of the largest received SINR at SU among all i usable beams. It is not difficult to see that

$$\gamma_{1:i}^{(S)} = \frac{P_{1:i}^{(S)}}{I_R^{(S)} + \sigma_S^2}, \tag{2.15}$$

where $P_{1:i}^{(S)}$ denotes the largest received power at SU among all i usable beam vectors, and $I_R^{(S)}$ denotes the interference from PT to SU, whose PDFs can be given by [29]

$$f_{I_R^{(S)}}(x) = \overline{I}_S e^{-\frac{x}{\overline{I}_S}}, \tag{2.16}$$

and

$$f_{P_{1:i}^{(S)}}(x) = \frac{i}{\overline{P}_S} e^{-\frac{x}{\overline{P}_S}} (1 - e^{-\frac{x}{\overline{P}_S}})^{i-1}, \tag{2.17}$$

where $\overline{I}_S$ denotes the average interference from PT to SU, and $\overline{P}_S$ denotes the average received power from SBS to SU, respectively. Therefore, the CDF of $\gamma_{1:i}^{(S)}$ can be calculated as

$$F_{\gamma_{1:i}^{(S)}}(x) = \Pr\left[\frac{P_{1:i}^{(S)}}{I_R^{(S)} + \sigma_S^2} < x\right] = \int_0^{\infty} \int_0^{(\overline{I}_S z + \sigma_S^2)x} f_{I_R^{(S)}}(z) f_{P_{1:i}^{(S)}}(y) dy dz. \tag{2.18}$$

[3]We assume that operation time required for proposed CUBS strategy is much less than channel coherence time, such that the effect on secondary throughput can be ignored.

By substituting (2.16) and (2.17) into (2.18), carrying out integrations and taking derivative, the PDF of $\gamma_{1:i}^{(S)}$ can be obtained as

$$f_{\gamma_{1:i}^{(S)}}(x) = \frac{d}{dx}F_{\gamma_{1:i}^{(S)}}(x) = \sum_{j=0}^{i}(-1)^{j+1}\binom{i}{j}e^{-\frac{j\sigma_S^2 x}{\overline{P}_S}}\frac{\frac{j\sigma_S^2}{\overline{P}_S}(1+\frac{\overline{I}_S}{\overline{P}_S}x)+\frac{\overline{I}_S}{\overline{P}_S}}{(1+\frac{\overline{I}_S}{\overline{P}_S}x)^2}. \quad (2.19)$$

After substituting (2.19) into (2.13) and manipulations, the exact average throughput of the secondary system for single SU case can be obtained as

$$\begin{aligned} R &= \sum_{i=1}^{M}\Pr[M_a=i]\sum_{j=0}^{M_a}(-1)^{j+1}\binom{M_a}{j}\int_0^{\infty}\log_2(1+x) \\ &\quad \left\{\frac{\frac{j\sigma_S^2}{\overline{P}_S}}{1+\frac{\overline{I}_S}{\overline{P}_S}x}+\frac{\frac{\overline{I}_S}{\overline{P}_S}}{(1+\frac{\overline{I}_S}{\overline{P}_S}x)^2}\right\}e^{-\frac{j\sigma_S^2 x}{\overline{P}_S}}dx. \end{aligned} \quad (2.20)$$

2.3.4 Outage Probability of the Primary System

The outage probability of the primary system is defined as the probability that the received SINR at PR, γ, is less than the predefined outage threshold γ_{th}, which can be calculated as

$$F(\gamma_{th}) = \sum_{i=0}^{M}\Pr[\gamma<\gamma_{th}, M_a=i], \quad (2.21)$$

where $\Pr[\gamma<\gamma_{th}, M_a=i]$ denotes the outage probability of the primary system when i beams are usable for transmission. For the case of $\gamma_{th}<\gamma_D$, the primary system is outage if and only if the SNR at PR is less than γ_{th}. Then (2.21) can be simplified as

$$F(\gamma_{th}) = \Pr\left[\frac{P_R}{\sigma_P^2}<\gamma_{th}\right] = 1-e^{-\frac{\sigma_P^2\gamma_{th}}{\overline{P}_R}}. \quad (2.22)$$

For the case of $\gamma_{th}\geq\gamma_D$, the outage probability is upper bounded by the worst case that the beam with the largest interference power at PR is always selected for

transmission, which can be given by

$$\begin{aligned}
F(\gamma_{th}) &\leq \sum_{i=1}^{M-1} \Pr\left[\frac{P_R^{(P)}}{I_{M-i+1:M}^{(P)}+\sigma_P^2} < \gamma_{th}, \frac{P_R^{(P)}}{I_{M-i+1:M}^{(P)}+\sigma_P^2} \geq \gamma_D, \frac{P_R^{(P)}}{I_{M-i:M}^{(P)}+\sigma_P^2} < \gamma_D\right] \\
&\quad + \Pr\left[\frac{P_R^{(P)}}{\sigma_P^2} < \gamma_{th}, \frac{P_R^{(P)}}{I_{M:M}^{(P)}+\sigma_P^2} < \gamma_D\right] + \Pr[\frac{P_R^{(P)}}{I_{1:M}^{(P)}+\sigma_P^2} < \gamma_{th}, \frac{P_R^{(P)}}{I_{1:M}^{(P)}+\sigma_P^2} \geq \gamma\Big] \\
&= \sum_{i=1}^{M-1} \Bigg\{ \int_{\gamma_{th}\sigma_P^2}^{\infty} \int_{\frac{s}{\gamma_{th}}-\sigma_P^2}^{\frac{s}{\gamma_D}-\sigma_P^2} \int_{\frac{s}{\gamma_D}-\sigma_P^2}^{\infty} f_{P_R^{(P)}}(s) f_{I_{M-i+1:M}^{(P)}, I_{M-i:M}^{(P)}}(y,z) ds dy dz \\
&\quad + \int_{\gamma_D\sigma_P^2}^{\gamma_{th}\sigma_P^2} \int_{0}^{\frac{s}{\gamma_D}-\sigma_P^2} \int_{\frac{s}{\gamma_D}-\sigma_P^2}^{\infty} f_{P_R^{(P)}}(s) f_{I_{M-i+1:M}^{(P)}, I_{M-i:M}^{(P)}}(y,z) ds dy dz \Bigg\} \\
&+ \int_0^{\gamma_{th}\sigma_P^2} \int_{\frac{s}{\gamma_{th}}-\sigma_P^2}^{\infty} f_{P_R^{(P)}}(s) f_{I_{M:M}^{(P)}}(x) ds dx + \int_0^{\infty} \int_{\gamma_D(x+\sigma_P^2)}^{\gamma_{th}(x+\sigma_P^2)} f_{P_R^{(P)}}(s) f_{I_{1:M}^{(P)}}(x) ds dx, \qquad (2.23)
\end{aligned}$$

where $f_{I_{1:M}^{(P)}}(x)$ and $f_{I_{M:M}^{(P)}}(x)$ are marginal PDFs of $I_{i:M}^{(P)}$, $f_{I_{M-i+1:M}^{(P)}, I_{M-i:M}^{(P)}}(x,y)$ is the joint PDF of $I_{M-i+1:M}^{(P)}$ and $I_{M-i:M}^{(P)}$, which have been given in (2.9), (2.10) and (2.11) , and $f_{P_R}(x)$ is the PDF of P_R, given by

$$f_{P_R}(x) = \frac{1}{\overline{P}_R} e^{-\frac{x}{\overline{P}_R}}, \qquad (2.24)$$

where $\overline{P}_R = \frac{P_P}{\Gamma d_P^{\lambda}}$ for notational conciseness. Finally, by substituting (2.9), (2.10), (2.11) and (2.24) into (2.23) and some manipulations, the close form expression of the upper bound of the outage probability can be calculated as

$$F(\gamma_{th}) \leq \begin{cases}
\sum_{i=1}^{M-1} \frac{M!}{i!} \sum_{n=0}^{M-i-1} \frac{(-1)^n}{n!(M-i-n-1)!} \Bigg\{ \Big[\frac{\Lambda\gamma_D}{(\Lambda\gamma_D+i)(\Lambda\gamma_D+i+n+1)} - \frac{e^{-\frac{i\sigma_P^2}{\overline{I}_P}(\frac{\gamma_{th}}{\gamma_D}-1)}}{\frac{i\gamma_{th}}{\gamma_D}+n+1+\Lambda\gamma_D} \\
+ \frac{e^{-\sigma_P^2(\frac{i}{\overline{I}_P}+\frac{\gamma_D}{\overline{P}_R})(\frac{\gamma_{th}}{\gamma_D}-1)}}{(1+\frac{\Lambda}{i}\gamma_D)(n+1+\Lambda\gamma_{th}+\frac{i\gamma_{th}}{\gamma_D})} \Big] e^{-\frac{\sigma_P^2\gamma_D}{\overline{P}_R}} + \Big[\frac{e^{-\frac{\sigma_P^2\gamma_D}{\overline{P}_R}}}{\Lambda\gamma_D+n+1+i\frac{\gamma_{th}}{\gamma_D}} - \frac{e^{-\frac{\sigma_P^2\gamma_{th}}{\overline{P}_R}}}{\Lambda\gamma_{th}+n+1+i\frac{\gamma_{th}}{\gamma_D}} \Big] \\
e^{-\frac{n\sigma_P^2(\frac{\gamma_{th}}{\gamma_D}-1)}{\overline{I}_P}} \Bigg\} + \sum_{n=0}^{M-1} (-1)^n \frac{M!}{n!(M-1-n)!} \Big\{ \frac{e^{-\frac{\sigma_P^2\gamma_D}{\overline{P}_R}}}{\Lambda\gamma_D+n+1} - \frac{e^{-\frac{\sigma_P^2\gamma_{th}}{\overline{P}_R}}}{\Lambda\gamma_{th}+n+1} \Big\} \\
+1 - e^{-\frac{\sigma_P^2\gamma_{th}}{\overline{P}_R} - \frac{M\sigma_P^2(\frac{\gamma_{th}}{\gamma_D}-1)}{\overline{I}_P}} - \frac{e^{-\frac{\gamma_D\sigma_P^2}{\overline{P}_R}}}{1+\frac{\Lambda}{M}\gamma_D} \Big\{ 1 - e^{-(\frac{M}{\overline{I}_P}+\frac{\gamma_D}{\overline{P}_R})(\frac{\gamma_{th}}{\gamma_D}-1)\sigma_P^2} \Big\}, & \gamma_{th} \geq \gamma_D; \\
1 - e^{-\frac{\sigma_P^2\gamma_{th}}{\overline{P}_R}}, & \gamma_{th} < \gamma_D.
\end{cases} \qquad (2.25)$$

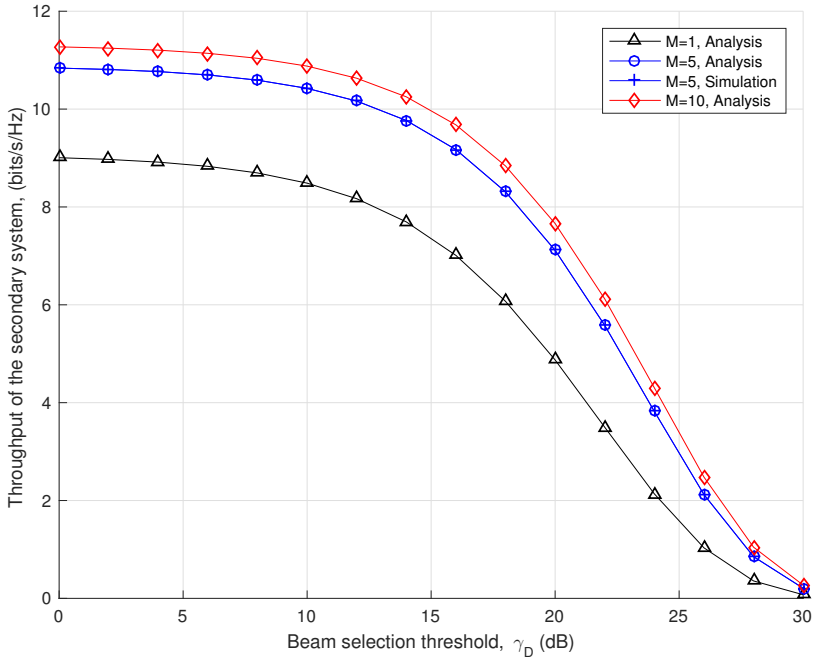

Figure 2.2: Throughput of the secondary system.

2.3.5 Numerical Examples

In Fig. 2.2, we plot the throughput of the secondary system as a function of the beam selection threshold γ_D for different beam number M. We can see that larger M leads to larger throughput, as the secondary system enjoys more diversity gain. We also observe with the increase of the beam selection threshold γ_D, the throughput of the secondary system gradually reduces to 0. This is because with larger γ_D, fewer usable beams will be fed back to the SBS, resulting in smaller diversity gain for the secondary system. We also compare analytical results with Monte Carlo simulation results for $M = 5$ case. We can see our analytical results perfectly match simulation results.

In Fig. 2.3, we plot the upper bound and simulated exact outage probability of the primary system as a function of outage threshold γ_{th} with $M = 5$ beams. We can see that when $\gamma_{th} \leq \gamma_D$, the curve follows exponential distribution; when $\gamma_D < \gamma_{th}$, the outage performance will suffer burst degradation. This is because the SBS may select the beam that leads to the received SINR at PR smaller than γ_{th} for transmission. We also observe that with known outage threshold γ_{th}, the increase of

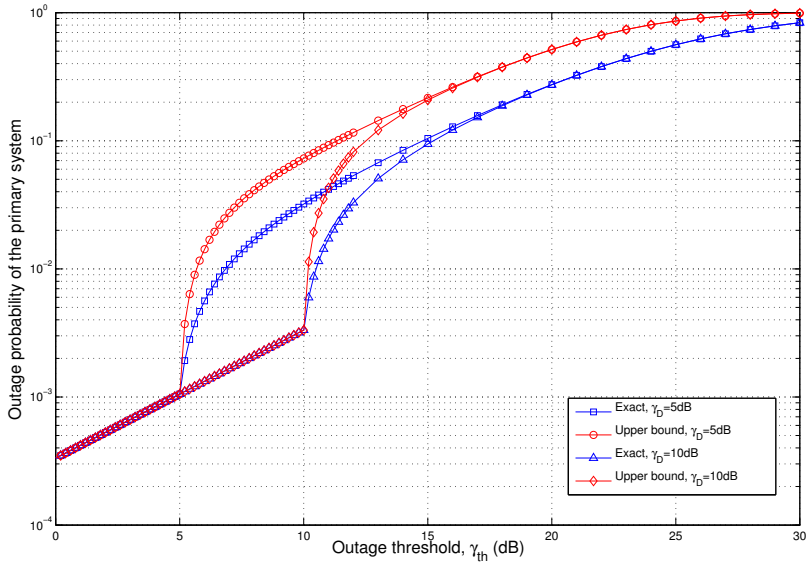

Figure 2.3: Outage probability of the primary system ($M = 5$).

γ_D can not affect the value of the outage probability, while reducing the throughput of the secondary system. Therefore, to avoid the burst increase of the outage probability of the primary system, as well as achieve the maximal throughput of the secondary system, the beam selection threshold should be equal to the outage threshold of the primary system.

2.4 Cooperative Active Beam Selection for Multiple SUs

For multiple SUs case ($K \geq M$), the SBS serves multiple selected SUs with multiple beam-forming vectors. Then PR will suffer interference from all active beams. To maximize its sum-rate, the SBS needs to select a maximal number of active beams to serve its SUs, while trying to ensure the received SINR at PR is above the SINR threshold γ_D. In this case, we consider two power allocation strategies for proposed beam selection scheme. In the first strategy, termed as constant beam power cooperative active beam selection (CBP-CABS) strategy, the transmission power on each beam remains constant regardless the number of active beams. With constant total power cooperative active beam selection (CTP-CABS) strategy, however, the total transmit power is equally allocated only to the active beams and, as such, the transmission power on each beam changes with the number of active beams.

2.4.1 CBP-CABS Strategy

At the beginning of each channel coherence time, PR estimates the received signal power P_R, and then sends it to the SBS. The SBS estimates the channel vector from the SBS to PR, and then calculates and ranks the projection amplitude square α_m for each beam, the order version of which is denoted by $\alpha_{m:M}$, where $\alpha_{1:M} \geq \alpha_{2:M} \geq \cdots \geq \alpha_{M:M}$. After that, the SBS calculates the received SINR at PR when the SBS uses the m best beams, i.e. the m beams that generate the least interference to PR, corresponding to $\alpha_{M-m+1:M}$ to $\alpha_{M:M}$. The total interference power at PR can be given by $\sum_{i=M-m+1}^{M} I_{i,m}^{(B)}$, where $I_{i,m}^{(B)}$ denotes the interference power from the ith best beam with beam power $\frac{P_S}{M}$, given by

$$I_{i,m}^{(B)} = \left(\frac{1}{\Gamma d_I^{\lambda}}\right)\left(\frac{P_S}{M}\right)\alpha_{i:M}, \quad i = M-m+1, \ldots, M. \tag{2.26}$$

Note that the transmit power on each beam is constant, independent of the number of active beams. Then the received SINR at PR, when m best beams are used for transmission, denoted by $\gamma_m^{(B)}$, can be given by

$$\gamma_m^{(B)} = \frac{P_R}{\sum_{i=M-m+1}^{M} I_{i,m}^{(B)} + \sigma_p^2}, \qquad 1 \le m \le M, \tag{2.27}$$

where σ_p^2 denotes the noise variance at PR. By substituting (2.1) and (4.24) into (2.27), we have

$$\gamma_m^{(B)} = \frac{\frac{P_P}{d_P^\lambda}|g|^2}{\frac{P_S}{Md_I^\lambda}\sum_{i=M-m+1}^{M}\alpha_{i:M} + \Gamma\sigma_p^2}, \quad 1 \le m \le M. \tag{2.28}$$

If the received SINR with m best beams is larger than the beam selection threshold γ_D, whereas the received SINR with $m+1$ best beams is less than γ_D, i.e. $\gamma_m^{(B)} \ge \gamma_D$ and $\gamma_{m+1}^{(B)} < \gamma_D$, the BS then uses the m best beams for transmission. It is worth noting that the received SINR at PR can be smaller than γ_D even when the BS uses the best beam only for transmission, i.e. the received SINR $\gamma_1^{(B)} < \gamma_D$. In this case, the SBS will hold transmission for a channel coherence time.

2.4.2 CTP-CABS Strategy

With CTP-CABS strategy, the total transmission power of SBS, P_S, is uniformly allocated only to those active beams. The total interference power at PR, when the m best beams are used, can be written as $\sum_{i=M-m+1}^{M} I_{i,m}^{(T)}$, where $I_{i,m}^{(T)}$ denotes the interference power from the ith best beam when m best beams are used for transmission, given by

$$I_{i,m}^{(T)} = \left(\frac{1}{\Gamma d_I^\lambda}\right)\left(\frac{P_S}{m}\right)\alpha_{i:M}, \quad i = M-m+1, \ldots, M. \tag{2.29}$$

Note that in this case the allocated power on each active beam is $\frac{P_S}{m}$. Then the received SINR at PR, when m best beams are used for transmission, can be given by

$$\gamma_m^{(T)} = \frac{\frac{P_P}{d_P^\lambda}|g|^2}{\frac{P_S}{md_I^\lambda}\sum_{i=M-m+1}^{M}\alpha_{i:M} + \Gamma\sigma_p^2}, \quad 1 \le m \le M. \tag{2.30}$$

Similar as CBP-CABS scheme, the SBS will use m selected beams for transmission if and only if $\gamma_m^{(T)} \geq \gamma_D$ and $\gamma_{m+1}^{(T)} < \gamma_D$, and hold transmission if $\gamma_1^{(T)} < \gamma_D$.

For both strategies, the SBS will perform random beamforming transmission [33, 34] with the selected beams.

2.4.3 Performance Analysis

Different values of γ_D will lead to different performance tradeoff between primary and secondary systems. In the following, we derive the closed-form expression of the outage probability for the primary system with both beam selection strategies.

Conditioning on the number of active beams used for transmission, denoted by N_a, the outage probability for CBP-CABS strategy can be represented as

$$P_{out}^{(B)}(\gamma_{th}) = \sum_{m=0}^{M} \Pr[\gamma_m^{(B)} < \gamma_{th}, N_a = m]. \tag{2.31}$$

According to the CBP-CABS strategy, the number of active beams N_a is equal to m $(1 \leq m < M)$ if and only if $\gamma_m^{(B)} \geq \gamma_D$, and $\gamma_{m+1}^{(B)} < \gamma_D$. Furthermore, the number of active beams N_a is equal to 0 if the SINR threshold requirement can not be satisfied with the best beam used for transmission i.e., $\gamma_1^{(B)} < \gamma_D$, and equal to M if the received SINR is larger than γ_D with all M beams active, i.e., $\gamma_M^{(B)} \geq \gamma_D$. Therefore, we can rewrite (2.31) as

$$\begin{aligned} P_{out}^{(B)}(\gamma_{th}) &= \sum_{m=1}^{M-1} \Pr\left[\gamma_m^{(B)} < \gamma_{th}, \gamma_m^{(B)} \geq \gamma_D, \gamma_{m+1}^{(B)} < \gamma_D\right] \\ &\quad + \Pr\left[\frac{P_R}{\sigma_p^2} < \gamma_{th}, \gamma_1^{(B)} < \gamma_D\right] + \Pr\left[\gamma_D \leq \gamma_M^{(B)} < \gamma_{th}\right]. \end{aligned} \tag{2.32}$$

For the case of $\gamma_{th} \leq \gamma_D$, (2.32) can be simply calculated as

$$P_{out}^{(B)}(\gamma_{th}) = \Pr\left[P_R < \sigma_p^2 \gamma_{th}\right] = \int_0^{\sigma_p^2 \gamma_D} f_{P_R}(x) dx, \tag{2.33}$$

where $f_{P_R}(x)$ denote the PDF of P_R, given by (2.24). By substituting (2.24) into (2.33), $P_{out}^{(B)}(\gamma_{th})$ can be calculated as

$$P_{out}^{(B)}(\gamma_{th}) = 1 - e^{-\frac{\sigma_p^2 \gamma_{th}}{P_R}}, \quad \gamma_{th} \leq \gamma_D. \tag{2.34}$$

For the case of $\gamma_{th} > \gamma_D$, (2.32) can be mathematically calculated as

$$\begin{aligned} P_{out}^{(B)}(\gamma_{th}) = \sum_{m=1}^{M-1} \int_0^\infty \int_0^\infty \int_{\gamma_D(y+\sigma_p^2)}^{\min(\gamma_D(y+z+\sigma_p^2),\gamma_{th}(y+\sigma_p^2))} f_{P_R}(x) \\ \times f_{\sum_{i=1}^m I_{i,m+1}^{(B)}, I_{m+1,m+1}^{(B)}}(y,z)dxdydz \\ + \int_0^\infty \int_0^{\min(\gamma_{th}\sigma_p^2, \gamma_D(y+\sigma_p^2))} f_{I_{1,1}^{(B)}}(y) f_{P_R}(x)dxdy \\ + \int_0^\infty \int_{\gamma_D(y+\sigma_p^2)}^{\gamma_{th}(y+\sigma_p^2)} f_{\sum_{i=1}^M I_{i,M}^{(B)}}(y) f_{P_R}(x)dxdy, \end{aligned} \tag{2.35}$$

where $f_{\sum_{i=1}^M I_{i,M}^{(B)}}(x)$, and $f_{I_{m+1,m+1}^{(B)}, \sum_{i=1}^m I_{i,m+1}^{(B)}}(x,y)$ denote the PDF of $\sum_{i=1}^M I_{i,M}^{(B)}$, and the joint PDF of $\sum_{i=1}^m I_{i,m+1}^{(B)}$ and $I_{m+1,m+1}$, respectively, the closed form expression of which can be obtained as [29]

$$f_{\sum_{i=1}^M I_{i,M}^{(B)}}(x) = \frac{x^{M-1} e^{-\frac{x}{\overline{P}_S}}}{\overline{P}_S^M (M-1)!}, \tag{2.36}$$

and

$$\begin{aligned} f_{\sum_{i=1}^m I_{i,m+1}^{(B)}, I_{m+1,m+1}^{(B)}}(x,y) &= \frac{M! e^{-\frac{x+(M-m)y}{\overline{P}_S}}}{m!(m-1)!(M-m-1)!\overline{P}_S^{m+1}} \\ &\times \sum_{j=0}^{m-1} \binom{m}{j} (-1)^j (x-jy)^{m-1} \mathcal{U}(x-jy), \quad x < my, \end{aligned} \tag{2.37}$$

respectively, where $\mathcal{U}(\cdot)$ denotes step function, and $\overline{P}_S = \frac{P_S}{M\Gamma d_I^\lambda}$ for notational conciseness. By substituting (2.24), (2.36) and (2.37) into (2.35) and carrying out integrations, we can obtain the closed form expression of $P_{out}^{(B)}(\gamma_{th})$ for CBP-CABS stratagy

as

$$P_{out}^{(B)}(\gamma_{th}) = \begin{cases} \sum_{m=1}^{M-1} \frac{M!}{(M-m)!(m-1)!(M-m-1)!\overline{P}_S^{M-m+1}} \sum_{i=0}^{M-m} \binom{M-m}{i}(-1)^i \Bigg\{ e^{-\frac{\gamma_D\sigma_p^2}{\overline{P}_R}} \\ \left[R_1\left(-\frac{m}{\overline{P}_S}, -\frac{1}{\overline{P}_S} - \frac{\gamma_D}{\overline{P}_R} \right) - R_2\left(-\frac{m}{\overline{P}_S} - \frac{\gamma_D}{\overline{P}_R}, -\frac{1}{\overline{P}_S} - \frac{\gamma_D}{\overline{P}_R} \right) \right] \\ -e^{-\frac{\gamma_{th}\sigma_p^2}{\overline{P}_R}} R_3\left(-\frac{m}{\overline{P}_S}, -\frac{1}{\overline{P}_S} - \frac{\gamma_{th}}{\overline{P}_R} \right) \Bigg\} + \frac{e^{-\frac{\gamma_D\sigma_p^2}{\overline{P}_R}}}{\left(1+\frac{\overline{P}_S\gamma_D}{\overline{P}_R}\right)^M} - \frac{e^{-\frac{\gamma_{th}\sigma_p^2}{\overline{P}_R}}}{\left(1+\frac{\overline{P}_S\gamma_{th}}{\overline{P}_R}\right)^M} \\ +1 - e^{-\frac{\gamma_{th}\sigma_p^2}{\overline{P}_R} - \frac{M\rho\sigma_p^2}{\overline{P}_S}} - \frac{e^{-\frac{\gamma_D\sigma_p^2}{\overline{P}_R}}}{1+\frac{\overline{P}_S\gamma_D}{M\overline{P}_R}} \left\{ 1 - e^{-\left(\frac{M}{\overline{P}_S}+\frac{\gamma_D}{\overline{P}_R}\right)\rho\sigma_p^2} \right\}, & \gamma_{th} > \gamma_D; \\ 1 - e^{-\frac{\sigma_p^2\gamma_{th}}{\overline{P}_R}}, & \gamma_{th} \le \gamma_D, \end{cases} \tag{2.38}$$

where

$$R_1(x,y) = \sum_{\lambda=0}^{M-m-1} (-1)^{1+\lambda} i^{M-m-1-\lambda} \frac{(M-m-1)!}{(M-m-1-\lambda)!} \sum_{t=0}^{\lambda} \frac{(M-m-1-t)!}{(\lambda-t)!y^{t+1}} \left\{ \frac{(M-m)^{\lambda-t}}{[x+y(M-m)]^{M-m-t}} - \frac{i^{\lambda-t}}{(x+yi)^{M-m-t}} \right\}, \tag{2.39}$$

$$\begin{aligned} R_2(x,y) = {} & R_1(x,y)\mathcal{U}\left(i-\frac{1}{\rho}\right) + \left\{ R_1(x,y) - S_1\left(x,y,\frac{\rho\sigma_p^2}{1-i\rho}\right) \right\} \left\{ \mathcal{U}\left(\frac{1}{\rho}-i\right) - \mathcal{U}\left(\frac{1}{\rho}-(M-m)\right) \right\} \\ & + \Bigg\{ S_2\left(x,y,\frac{\rho\sigma_p^2}{1-(M-m)\rho}\right) + R_1(x,y) - \Bigg[S_1\left(x,y,\frac{\rho\sigma_p^2}{1-i\rho}\right) \\ & - S_1\left(x,y,\frac{\rho\sigma_p^2}{1-(M-m)\rho}\right) \Bigg] \Bigg\} \mathcal{U}\left(\frac{1}{\rho}-(M-m)\right), \end{aligned} \tag{2.40}$$

and

$$\begin{aligned} R_3(x,y) = {} & S_1\left(x,y,\frac{\rho\sigma_p^2}{1-i\rho}\right) \left\{ \mathcal{U}\left(\frac{1}{\rho}-i\right) - \mathcal{U}\left(\frac{1}{\rho}-(M-m)\right) \right\} + \Bigg\{ S_1\left(x,y,\frac{\rho\sigma_p^2}{1-i\rho}\right) \\ & - S_1\left(x,y,\frac{\rho\sigma_p^2}{1-(M-m)\rho}\right) - S_2\left(x,y,\frac{\rho\sigma_p^2}{1-(M-m)\rho}\right) \Bigg\} \mathcal{U}\left(\frac{1}{\rho}-(M-m)\right), \end{aligned} \tag{2.41}$$

where

$$S_1(x,y,z) = \sum_{\lambda=0}^{M-m-1} (-i)^{M-m-1-\lambda} \frac{(M-m-1)!}{(M-m-1-\lambda)!} \sum_{t=0}^{\lambda} \frac{(-1)^t}{(\lambda-t)! y^{t+1}}$$
$$\left\{ \sum_{j=0}^{M-m-1-t} (-1)^j \frac{(M-m-1-t)!}{(M-m-1-t-j)!} \right.$$
$$\frac{z^{M-m-1-t-j} i^{\lambda-t} e^{(x+iy)z}}{(x+iy)^{j+1}} - e^{-\sigma_p^2 y} \sum_{s=0}^{\lambda-t} \frac{(-\sigma_p^2)^{\lambda-t-s}}{\rho^s} \binom{\lambda-t}{s}$$
$$\left. \sum_{j=0}^{M-m-1-\lambda+s} (-1)^j \frac{(M-m-1-\lambda+s)!}{(M-m-1-\lambda+s-j)!} \frac{z^{M-m-1-\lambda+s-j} e^{(x+\frac{y}{\rho})z}}{(x+\frac{y}{\rho})^{j+1}} \right\}, \quad (2.42)$$

and

$$S_2(x,y,z) = \sum_{\lambda=0}^{M-m-1} \frac{(M-m-1)!(-i)^{M-m-1-\lambda}}{(M-m-1-\lambda)!} \sum_{t=0}^{\lambda} \frac{(-1)^t}{(\lambda-t)! y^{t+1}}$$
$$\sum_{j=0}^{M-m-1-t} \frac{(M-m-1-t)!(-1)^j z^{M-m-1-t-j}}{(M-m-1-t-j)!}$$
$$\left\{ \frac{(M-m)^{\lambda-t} e^{(x+y(M-m))z}}{[x+y(M-m)]^{j+1}} - \frac{i^{\lambda-t} e^{(x+yi)z}}{(x+yi)^{j+1}} \right\}, \quad (2.43)$$

where $\rho = \frac{\gamma_{th}}{\gamma_D} - 1$. Note that the outage probability for CTP-CABS strategy can also be obtained by following similar procedure as CBP-CABS strategy, which is omitted here due to space limitation.

In Fig. 2.4, we plot the outage probability of the primary system as a function of the outage threshold γ_{th} for $M = 2$ antennas. We can observe that for the case of $\gamma_{th} \leq \gamma_D$, the primary system has the same outage probability as no interference case. For the case of $\gamma_{th} > \gamma_D$, the outage probability of the primary system will suffer burst degradation. This is because the secondary system may transmit with beams that lead to the received SINR at PR below γ_{th}. We can also observe that the outage performance for CBP-CABS strategy is slightly better than CTP-CABS strategy when γ_{th} is small, and worse when γ_{th} is larger. When γ_{th} is very large, the difference between the outage probability of these two strategies disappears.

In Fig. 2.5, we plot the average sum-rate of the secondary multiuser MIMO system as a function of the beam selection threshold γ_D for different user number K for $M = 2$ antennas, assuming the user selection scheme proposed in [35] is used. According to [35], each secondary user feeds back its best beam index and the corresponding SINR value to the secondary base station. For example, if the mth beam leads to the largest

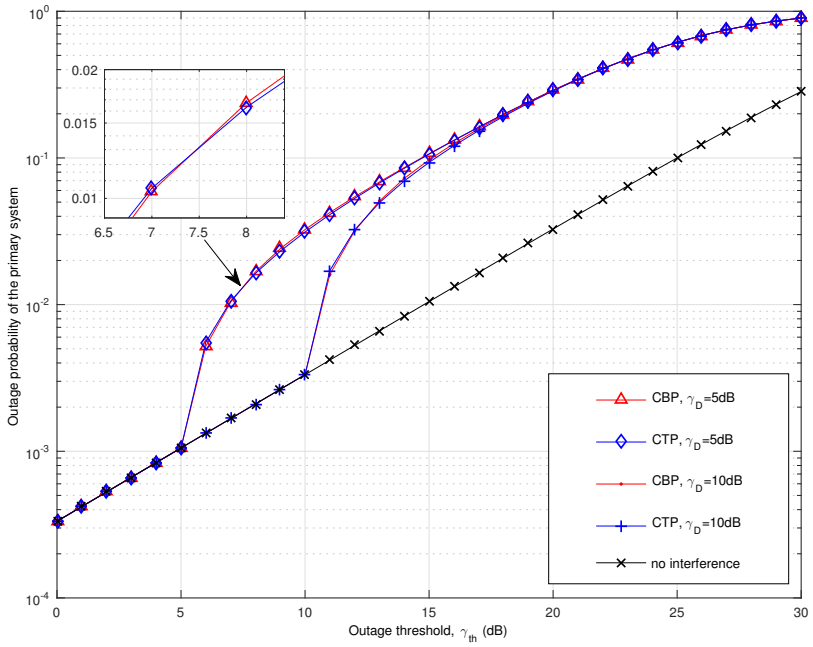

Figure 2.4: Outage probability of the primary system ($M = 2$).

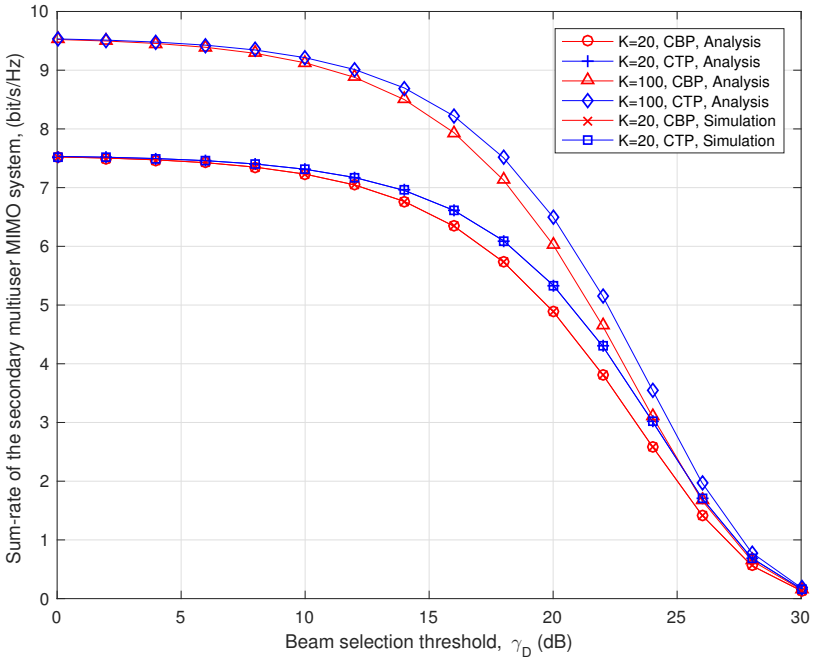

Figure 2.5: Sum-rate of the secondary multiuser MIMO system.

SINR for the kth user, then the kth user will feedback the beam index m and the corresponding SINR value $\gamma_{k,m}$. Based on the feedback information, the secondary base station assigns a beam to the user with the largest SINR value among all users who feed back the index of that beam. Specifically, the base station ranks all K feedback best beam SINRs. If $\gamma_{k,m}$ is the largest one among all K SINRs, then the base station selects the kth user for the mth beam. After that, the base station will rank the feedback SINRs for the remaining beams. If now $\gamma_{n,l}$ is the largest one, where $l \neq m$ and $n \neq k$, then the base station assigns the lth beam to the nth user. This process is continued until either all beams have been assigned to selected users or there are some unrequested beams remaining. In the later case, the secondary base station will randomly select users for the remaining beams. The ergodic sum rate of the resulting system, when N_a beams are available, is given by

$$R_{N_a} = \mathbf{E}_{\{\gamma_{B_m}\}_{m=1}^{N_a}} \left\{ \sum_{m=1}^{N_a} \log_2(1+\gamma_{B_m}) \right\}, \tag{2.44}$$

where γ_{B_m} is the received SINR of the selected user on the mth beam.

We can observe that with the increase of γ_D, the sum-rate of the secondary system gradually reduces to 0, as expected by intuition. The CTP-CABS strategy always leads to larger sum-rate than CBP-CABS strategy. Therefore, to avoid the burst increase of the outage probability of the primary system, as well as achieve the maximal sum-rate of the secondary system, the beam selection threshold γ_D should be equal to the outage threshold γ_{th}. The CTP-CABS strategy should be used to improve secondary system sum-rate performance. We also compare analytical results with Monte Carlo simulation results for $K = 20$ case. We can see our analytical results perfectly match simulation results.

2.5 Concluding Remarks

We proposed cooperative beam selection strategies to regulate the received SINR for the primary system while achieving the maximal sum-rate for the secondary system. For single SU case, we proposed a cooperative usable beam selection (CUBS) strategy, where PR only needs to feed back to the secondary system the received signal power from the PT to PR, based on which the SBS calculates the received SINR at PR for each beam, and decides usable beams that lead to the received SINR at PR larger

than a predefined threshold. We derive the upper bound expression of the outage probability for the primary system and throughput for the secondary system. For multiple SUs case, we proposed two cooperative beam selection strategies, termed as CBP-CABS and CTP-CABS, to select a maximal number of beams that the secondary multiuser MIMO system can use while satisfying the received SINR requirement at PR. We also analyzed the exact outage performance of the primary system for each strategy, and investigated the tradeoff between primary system outage probability versus secondary system sum-rate performance. The result shows that CTP-CABS strategy can achieve larger sum-rate for the secondary system without significantly affecting the outage performance of the primary system.

Chapter 3

Performance of Overlaid Wireless Sensor Transmission with RF Energy Harvesting

3.1 Introduction

Wireless sensors are used in a wide range of applications, such as environment monitoring, surveillance, health care, intelligent buildings and battle field control [1]. The sensor nodes are usually powered by batteries with finite life time, which manifests as an important limiting factor to the functionality of wireless sensor network (WSN). Replacing or charging the batteries may either incur high costs for human labor or be impractical for certain application scenarios (e.g. applications that require sensors to be embedded into structures). Powering sensor nodes through ambient energy harvesting has therefore received a lot of attentions in both academia and industrial communities [2, 3]. Various techniques have been developed to harvest energy from conventional ambient energy sources, including solar power, wind power, thermoelectricity, and vibrational excitations [4, 5, 6, 7].

RF energy is another candidate ambient energy source for powering sensor nodes. Recently, there has been a growing interest in RF energy harvesting due to the intensive deployment of cellular/WiFi wireless systems in addition to traditional radio/TV broadcasting systems [8]. It has been experimentally proved that RF energy harvesting is feasible from the hardware implementation viewpoint. In [9], the authors developed prototypes for devices that communicate with each other using ambient

RF signals from TV/cellular systems as the only power source. In [10], the authors present the experimental performance (e.g., charging time of the sensor and received signal power at the sink) of RF energy harvesting using PowerCast energy harvesters [11]. Although these previous works have proved a visible future for the wireless applications based on RF energy harvesting, most performance results are obtained through laboratory experiments. There is still a lack of effective theoretical models that can analytically predict the performance of WSNs powered by RF energy harvesting.

In this Chapter, we consider an overlaid sensor transmission scenario where a sensor-to-sink communication link operates in the coverage of an existing wireless system over the same frequency. Unlike conventional WSN implementation, where both the sensor and the sink are equipped with reliable power supplies, we assume that only the sink has a constant power source and that the sensor needs to harvest RF energy from the transmission of existing wireless system. Specifically, the sensor node can only harvest RF energy when its received signal power is larger than a certain sensitivity level [25]. As such, the existing system, being either cellular, WiFi or TV broadcasting systems, serves as the ambient source for sensor energy harvesting and as interference source during sensor transmission. Such an overlaid implementation strategy of RF-energy powered WSN has the potential to offer attractive and green solutions to a wide range of sensing applications, particularly in view of the increasingly severe spectrum scarcity. While scavenging the radiated RF energy from existing system, the RF energy powered sensor transmission will introduce very limited interference to existing systems, due to its low transmission power and short transmission duration.

In this work, we investigate the packet transmission performance of the sensor-to-sink link over Rayleigh fading wireless channels. Considering sensor's limited energy harvesting capability, we assume that the link is used to support low-rate sensing applications with low traffic intensity. Specifically, we first consider delay sensitive scenario, where the sensor needs to periodically transmit a new packet to the sink with hard delay constraint. We evaluate the packet loss probability assuming no retransmission is allowed. For delay insensitive traffic, where the sensing data must be delivered to the sink without error at the expense of a certain delay, we calculate the average delay of packet transmission over the link with harvested energy. Whenever feasible, we derive the exact analytical expression for performance metrics of interest in simple closed form, which facilitates fast evaluation and convenient applications

to parameter optimization. These analytical results will help determine what type of sensing applications that the proposed overlaid sensor implementation strategy with RF energy harvesting can effectively support.

The main contributions of this chapter can be summarized as follows.

- We characterize the RF energy harvesting capability of wireless sensor node over Rayleigh fading channels over multiple channel coherence time. Especially, the statistical distribution of the amount of energy that can be harvested over a fixed number of channel coherence time is derived with the consideration of energy harvesting sensitivity and efficiency.

- We study the packet loss probability of delay sensitive traffic, which is dependent on the amount of harvested energy as well as the interference amount experienced during packet transmission. We examine the effect of traffic intensity and the energy storage capacity at the sensor on the packet loss probability based on the exact analytical results.

- For the case of delay insensitive traffic, we propose two low-complexity transmission strategies, depending upon whether the channel quality information of the sensor-to-sink link, in terms of the received signal-to-interference-plus-noise ratio (SINR), is available or not. When the received SINR information is not available at the sensor, we present a stop-and-wait type retransmission strategy to guarantee successful packet delivery for low-intensity delay-insensitive traffic. We also explore the available SINR information to adaptively transmit the packet only when the channel quality is acceptable, which leads to more effective utilization of the harvested RF energy.

- We carry out accurate average delay analysis with both transmission strategies for delay insensitive traffic. We derive the statistical distribution of the number of coherence time needed for fully charging the sensor. For the channel aware transmission strategy, we also derived the exact distribution of total transmission delay. Finally, we apply the analytical results to investigate the optimal sensor node design to minimize the average packet transmission delay.

The remainder of the Chapter is organized as follows. In Section 3.2, we introduce the system and channel model under consideration. The performance of the proposed sensing implementation for delay sensitive traffic is evaluated in Section

3.3. In Sections 3.4 and 3.5, we present and study two transmission strategies for delay insensitive traffic. Concluding remarks are given in Section 3.6.

3.2 System and Channel Model

3.2.1 System Model

We consider the point-to-point packet transmission from a single-antenna wireless sensor to its sink over a flat Rayleigh fading channel. The sink and the sensor are deployed in the coverage area of an existing wireless system, which could be cellular, WiFi or TV broadcasting systems. We assume that the sensor can harvest RF energy from the transmitted signal of the existing system, and use it as its sole energy source for transmission, as illustrated in Fig. 3.1.

We assume that the sensor works in two stages within one duty cycle, i.e., energy harvesting stage and packet transmission stage. [1] In the energy harvesting stage, the sensor harvests RF energy from the radio transmission of existing wireless systems over multiple channel coherence time. Typically, the sensor can harvest RF energy only when the received signal power is larger than a power threshold, denoted by P_{th} [25]. In general, P_{th} should be greater than the receiver sensitivity for information reception.

During the packet transmission stage, the sensor will transmit its collected information to the sink using harvested energy. We assume that the energy consumed for information collection is negligible compared with the energy used for transmission [28]. Then the energy that can be used for transmission is approximately equal to the harvested energy. Also note that the sensor transmission will suffer interference from the existing system in this stage, the effect of which will be further discussed in the following sections. Due to the low transmission power and short transmission duration, we ignore the interference that the sensor transmission may generate to the existing system.

We assume that basic sensor network setup in [9] (e.g., access control method, channel occupancy) is adopted in our paper, where the delay for access control and/or carrier sensing is ignorable compared with energy harvesting duration.

[1] Energy harvesting stage and packet transmission stage may correspond to sleep stage and wake up stage, respectively, for traditional wireless sensors.

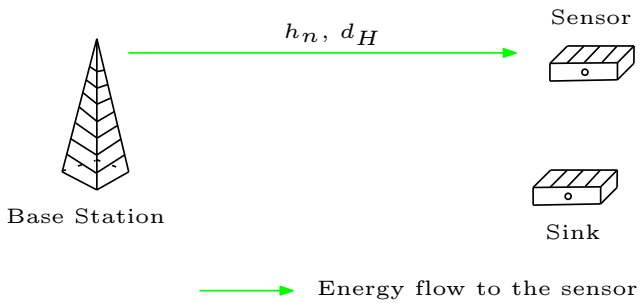

(a) Energy Harvesting Stage

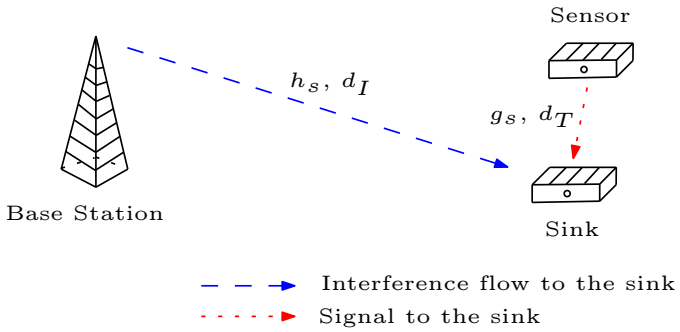

(b) Packet Transmission Stage

Figure 3.1: System model for two-stage sensor transmission with RF energy harvesting.

3.2.2 Channel Model

We adopt a log-distance path loss plus Rayleigh block fading channel models for the operating environment [30] while ignoring the shadowing effect for the sake of presentation clarity. In particular, the channel gain between the BS and the sensor remains constant over one channel coherence time, denoted by T_c, and changes to an independent value afterwards. Let h_n denote the fading channel gain over the nth coherence time, where $h_n \in \mathcal{CN}(0,1)$. For notational conciseness, we use α_n to denote its amplitude square, i.e. $\alpha_n = ||h_n||^2$, whose PDF for Rayleigh fading channel under consideration is given by

$$f_{\alpha_n}(x) = e^{-x}. \tag{3.1}$$

Then the instantaneous received signal power at the sensor over the nth coherence time is given by $P_n = \overline{P}\alpha_n$, where $\overline{P}$ is the average received power at the sensor due to path loss, given by

$$\overline{P} = \frac{P_T}{\Gamma d_H^{\lambda}}, \tag{3.2}$$

where P_T is the constant transmission power of BS, d_H is the distance from BS to the sensor, λ is the path loss exponent of the environment, ranging from 2 to 5, and Γ is a constant parameter of the log-distance path loss model. Specifically, $\Gamma = \frac{PL(d_0)}{d_0^{\lambda}}$, where d_0 is a reference distance of the antenna far field, and $PL(d_0)$ is linear path loss at distance d_0, depending on the propagation environment.

We assume, as is the case in real world systems [10][11], the sensor can only harvest energy when the instantaneous received signal power P_n is greater than the sensitivity level P_{th} and the harvested energy is proportional to $P_n - P_{th}$. Consequently, the amount of energy that the sensor can harvest during the nth coherence time can be represented as [25]

$$E_n = \begin{cases} \eta T_c(P_n - P_{th}), & P_n \geq P_{th}; \\ 0, & P_n < P_{th}, \end{cases} \tag{3.3}$$

where $0 \leq \eta \leq 1$ is RF energy harvesting efficiency. It follows that the amount of

energy harvested by the sensor over N consecutive coherence time can be given by

$$E_h^{(N)} = \min\left(\sum_{n=1}^{N} E_n, E_c\right), \tag{3.4}$$

where E_c is the energy storage capacity of the sensor. [2]

The transmission power of the sensor when it uses the harvested energy over N coherence time is equal to $\frac{E_h^{(N)}}{T_s}$, where T_s denotes the transmission time duration. We assume, with the notion of low-rate sensing applications, that T_s is much smaller than the channel coherence time T_c. Let h_s and g_s denote the fading channel gains from BS to the sink and from the sensor to the sink, respectively, where $h_s \in \mathcal{CN}(0,1)$ and $g_s \in \mathcal{CN}(0,1)$. The received SINR at the sink can be calculated as

$$\gamma_s = \frac{\frac{E_h^{(N)}}{T_s d_T^{\lambda}}||g_s||^2}{\frac{P_T}{d_I^{\lambda}}||h_s||^2 + \Gamma\sigma^2}, \tag{3.5}$$

where d_T is the distance from the sensor to the sink, d_I is the distance from BS to the sink, and σ^2 is the variance of the additive noise at the sink. In general, the sensor and the sink are very close to each other, i.e. $d_T \ll d_H \approx d_I$.

In the following, we study the performance of such overlaid sensor transmission when it is used to support low-rate data traffics. These analytical results can help design and optimize various system parameters, such as the number of channel coherence time for energy harvesting, N, sensor transmission power, etc. In this paper, we focus on properly designing energy storage capacity E_c, while assuming system parameters, such as BS transmit power P_T, sensor sensitivity P_{th}, sensor energy harvesting efficiency η, transmission time duration T_s, and channel model parameters to be fixed.

[2] E_c can also be viewed as the energy threshold, above which the sensor can carry out packet transmission. We will examine the optimization of this important design parameter in the following sections.

3.3 Performance Analysis for Delay Sensitive Traffic

We first consider delay sensitive traffic in this section. For certain sensing applications, such as smart metering and environment monitoring, the sensor node needs to periodically send their collected information (e.g. energy usage, temperature, humid information) to the sink. Any delay in the delivery of these information may render them useless. Therefore, the goal is to successfully transmit these information packet within a fixed time duration. As such, an important performance metric for such application is the packet loss probability, i.e. the percent of packets that could not be delivered to the sink in time. We now analyze the packet loss probability of the proposed overlaid sensing implementation with RF energy harvesting. An accurate quantification of this metric will help determine the sensing applications that could be supported with the proposed implementation.

3.3.1 Packet Loss Probability Analysis

We assume that the sensor must collect and transmit one packet to the sink over a fixed time duration T_F. The number of coherence time in T_F, denoted by N, is approximately equal to $\lfloor \frac{T_F}{T_c} \rfloor$. The sensor will first harvest RF energy for N channel coherence time and then transmit the packet to the sink using the harvested energy. We focus on low rate sensing application and ignore the potential packet collision with other sensors. We also assume that, with adoption of certain error correction coding scheme, the packet can be successfully received by the sink if the received SINR at the sink during packet transmission is above γ_T. As such, packet loss will occurs if and only if the received SINR at the sink during packet transmission is below the threshold γ_T. This may be due to insufficient harvested energy, poor sensor to sink channel quality, as well as strong interference from BS. Mathematically, the packet loss probability of the sensor transmission is given by

$$P_{PL} = \Pr[\gamma_s < \gamma_T] = \Pr[\frac{\frac{E_h^{(N)}}{T_s d_T^{\lambda}} ||g_s||^2}{\frac{P_T}{d_I^{\lambda}} ||h_s||^2 + \Gamma\sigma^2} < \gamma_T]. \tag{3.6}$$

Conditioning on $E_h^{(N)}$, the packet loss probability can rewritten in terms of the PDFs of $E_h^{(N)}$, $||g_s||^2$, and $||h_s||^2$, denoted by $f_{E_h^{(N)}}(\cdot)$, $f_{||g_s||^2}(\cdot)$, and $f_{||h_s||^2}(\cdot)$, respectively,

as

$$P_{PL} = \int_0^{E_c}\int_0^{\infty} F_{||g_s||^2}\left(\frac{T_s\gamma_T d_T^{\lambda}(\frac{P_T y}{d_I^{\lambda}}+\Gamma\sigma^2)}{z}\right) f_{||h_s||^2}(y) f_{E_h^{(N)}}(z)dydz. \quad (3.7)$$

The PDF of $||h_s||^2$ and $||g_s||^2$ for the Rayleigh fading channel model under consideration are commonly given by

$$f_{||h_s||^2}(x) = f_{||g_s||^2}(x) = e^{-x}. \quad (3.8)$$

After proper substitution and some manipulations, we can rewrite P_{PL} as

$$P_{PL} = \int_0^{E_c}\left(1 - \frac{ze^{-\frac{T_s\gamma_T\Gamma d_T^{\lambda}\sigma^2}{z}}}{z+\frac{P_T}{d_I^{\lambda}}T_s\gamma_T d_T^{\lambda}}\right) f_{E_h^{(N)}}(z)dz. \quad (3.9)$$

To proceed further, we need the PDF of the harvested energy over N coherence time, $f_{E_h^{(N)}}(z)$. In the Appendix A, we derive the close form expression of $f_{E_h^{(N)}}(x)$ as

$$f_{E_h^{(N)}}(x) =$$

$$\begin{cases} \sum_{i=2}^{N} \frac{N!(1-e^{-\frac{P_{th}}{\overline{P}}})^{N-i}e^{-\frac{x}{\eta T_c\overline{P}}-\frac{iP_{th}}{\overline{P}}}}{(i-1)!(i-2)!(N-i)!}\sum_{m=0}^{i-2}(1-i)^{i-2-m}C_{i-2}^{m} \\ \sum_{j=0}^{m}\frac{m!}{(m-j)!}\Big\{(i-1)^{m-j}\sum_{k=0}^{i-2-j}\frac{(i-2-j)!}{(i-2-j-k)!i^{k+1}}(\frac{x}{i\eta T_c\overline{P}}+\frac{P_{th}}{\overline{P}})^{i-2-j-k-1} \\ (\frac{x}{i\eta^2T_c^2\overline{P}^2}+\frac{P_{th}}{\eta T_c\overline{P}^2}-\frac{i-2-j-k}{i\eta T_c\overline{P}})+\sum_{s=0}^{m-j}(-1)^{m-j-s}C_{m-j}^{s}\frac{i^s}{i-1-j-s} \\ \Big\{(\frac{x}{i\eta T_c\overline{P}}+\frac{P_{th}}{\overline{P}})^{i-2-j}(\frac{x}{i\eta^2T_c^2\overline{P}^2}+\frac{P_{th}}{\eta T_c\overline{P}^2}-\frac{i-1-j}{i\eta T_c\overline{P}}) \\ +(\frac{P_{th}}{\overline{P}})^{i-1-j-s}(\frac{x}{i\eta T_c\overline{P}}+\frac{P_{th}}{\overline{P}})^{s-1}(-\frac{x}{i\eta^2T_c^2\overline{P}^2}-\frac{P_{th}}{\eta T_c\overline{P}^2}+\frac{s}{i\eta T_c\overline{P}})\Big\}\Big\} \\ +\frac{N}{\eta T_c\overline{P}}(1-e^{-\frac{P_{th}}{\overline{P}}})^{N-1}e^{-\frac{x}{\eta T_c\overline{P}}-\frac{P_{th}}{\overline{P}}}+(1-e^{-\frac{P_{th}}{\overline{P}}})^{N}\delta(x) \\ +\big[1-F_{E_h}(E_c)\big]\delta(x-E_c), & N>1; \\ \frac{1}{\eta T_c\overline{P}}e^{-\frac{x}{\overline{P}\eta T_c}-\frac{P_{th}}{\overline{P}}}+(1-e^{-\frac{P_{th}}{\overline{P}}})^{N}\delta(x)+\big[1-F_{E_h}(E_c)\big]\delta(x-E_c), & N=1, \end{cases} \quad (3.10)$$

where $\delta(\cdot)$ denotes the impulse function. The PDF of harvested energy over $N = 1, 2, 3$ coherence time is plotted in Fig. 3.2. We can see that $E_h^{(N)}$ follows a mixed distribution with impulse at $x = 0$ and $x = E_c$, which represents the probability that the sensor can not harvest any energy over N coherence time and the probability that the sensor will be fully charged after N coherence time. With the increase of the number of coherence time N, the continuous portion of probability mass moves

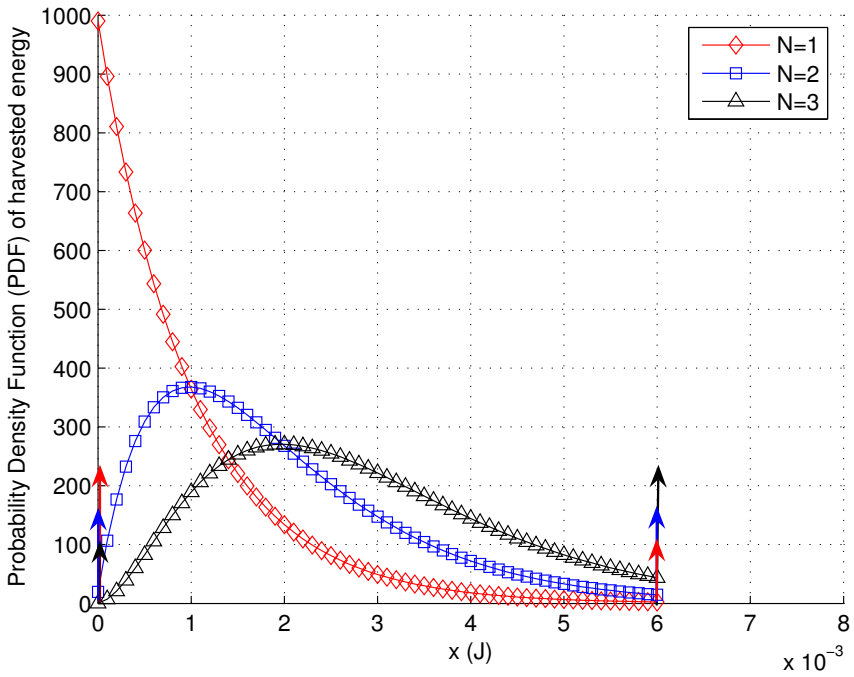

Figure 3.2: Distribution of harvested energy over N channel coherence time ($E_c = 0.006J$).

towards right, with the distribution of harvested energy spreads more widely along the energy axis. This is because when N increases, the sensor has larger probability to harvest more energy.

Finally, the packet loss probability for delay sensitive traffic can be calculated by substituting (3.10) into (3.9) and carrying out numerical integration. Note that only finite integration of some basic functions are involved in the calculation.

3.3.2 Numerical Results

We assume the same parameters for RF energy harvesting system as in [9]. In particular, the transmission power of BS is $P_T = 10kW$. The distance from BS to the sensor, BS to the sink and the sensor to the sink are set as $d_H = 100$ meters, $d_I = 100$ meters and $d_T = 1$ meter, respectively. The pass loss exponent λ is assumed to be 3, the channel coherence time T_c be $100ms$, and the transmission time of the sensor T_s be $1ms$. The sensitivity of the sensor is assumed to be $P_{th} = -10dBm = 0.1mW$ [10]. For simplicity, we assume harvesting efficiency $\eta = 1$ and path loss constant $\Gamma = 1$.

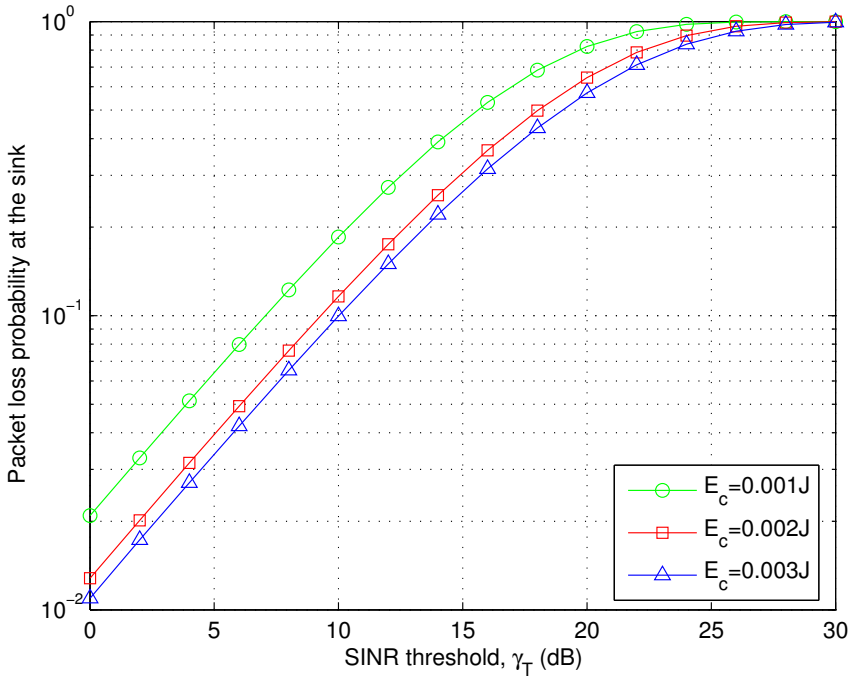

Figure 3.3: Packet loss probability at the sink for different energy storage capacity ($N = 3$).

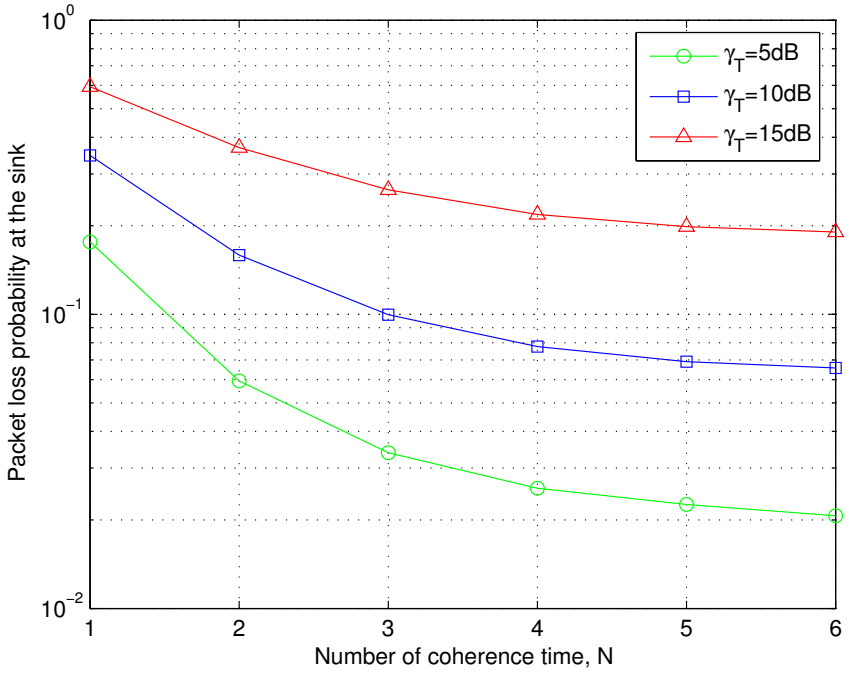

Figure 3.4: Packet loss probability at the sink over N coherence time.

In Fig. 3.3, we plot the packet loss probability at the sink as a function of the SINR threshold for different energy capacity E_c with $N = 3$. We can see when γ_T is small, the packet loss probability shows approximately linear degradation. We also observe that larger energy capacity E_c leads to smaller packet loss probability. However, the benefit of packet loss probability shrinks with the increase of the energy capacity E_c. This is because when E_c gets larger, the sensor has smaller probability to be fully charged, such that the effect of the energy capacity on the packet loss probability gradually reduces.

In Fig. 3.4, we plot the packet loss probability at the sink as a function of the number of the channel coherence time before each packet transmission. We can see the packet loss probability at the sink gradually reduces as N increases, and converge to a constant value when N is very large. This is due to the existence of energy storage capacity E_c, which limits the total harvested energy and in turn the transmission power. Moreover, we notice that higher SINR threshold leads to higher packet loss probability, as expected by intuition. Note that our analysis results accurately reflect *how* the packet loss probability decreases with the increase of energy harvesting time NT_c, which can be used to predict whether the packet loss probability requirement can be satisfied with a given maximum delay requirement NT_c.

3.4 Channel-Blind Transmission Strategy for Delay insensitive Traffic

We now consider the transmission of delay insensitive traffic with the proposed overlaid sensing implementation with RF energy harvesting. We focus on low-intensity traffic, whose packets need to be delivered to the sink reliably while suffering certain delay. The delay insensitive traffic applies to the sensing scenarios that require high-level data integrity but are less time-critical. The performance metric of primary interest becomes the average delay for packet delivery, which for the sensor transmission with energy harvesting include the energy harvesting time as well as transmission delay.

In this section, we adopt a channel blind transmission strategy where the sensor will transmit the packet immediately after being fully charged, i.e. harvesting at least E_c amount of energy. If the transmission is not successful, the sensor will restart the energy harvesting and packet transmission process until the packet is successfully

received. We analyze the average delay performance for packet delivery with the channel blind strategy in the following. We first derive the distribution of the time required to fully charge the sensor, based on which we obtain the exact closed-form expression on the average packet transmission delay with retransmission. We also investigate the effect of energy storage capacity E_c on the average packet delivery delay and its optimization. We ignore the queuing delay in the analysis in this work since our focus is on sensing applications with low traffic intensity. The results here can however be applied to the queuing delay analysis of high-intensity traffic by adopting certain queuing models.

3.4.1 Distribution of Charging Time

We first derive the statistics of the charging time, i.e. the number of T_c that it takes to fully charge the sensor. Let $\Pr[T_d = KT_c]$ denote the probability that the sensor can be fully charged in K channel coherence time, which is equal to the probability that the harvested energy during the first $K-1$ coherence time is less than E_c, and that during first K coherence time larger than E_c.[3] Therefore, we can calculate $\Pr[T_d = KT_c]$ as

$$\begin{aligned}\Pr[T_d = KT_c] &= \Pr[\sum_{j=1}^{K-1} E_j + E_K \geq E_c, \sum_{j=1}^{K-1} E_j < E_c] \\ &= \int_0^{E_c} \int_{E_c - z}^{E_c} f_{E_h^{(1)}}(z) f_{E_h^{(K-1)}}(x) dx dz, \end{aligned} \tag{3.11}$$

where $f_{E_h^{(1)}}(x)$ denotes the PDF of the harvested energy in one coherence time, and $f_{E_h^{(K-1)}}(x)$ denoted the PDF of the harvested RF energy distribution over the first $K-1$ coherence time, both of which can be obtained from (3.10). After carrying out integration and some manipulation, the close form expression of $\Pr[T_d = KT_c]$ is

[3]Random walk theory or Brownian motion can not be used here, as the distribution of harvested energy over one coherence is mixed with impulse at 0 and E_c.

given by

$$\Pr[T_d = KT_c] \;=$$

$$\begin{cases} e^{-\frac{E_c}{\overline{P}\eta T_c}-\frac{P_{th}}{\overline{P}}} \sum_{i=2}^{K-1} \frac{(K-1)!(1-e^{-\frac{P_{th}}{\overline{P}}})^{K-1-i} e^{-\frac{iP_{th}}{\overline{P}}}}{(i-1)!(i-2)!(K-1-i)!} \sum_{m=0}^{i-2}(1-i)^{i-2-m} \\ C_{i-2}^{m} \sum_{j=0}^{m} \frac{m!}{(m-j)!} \Bigg\{ (i-1)^{m-j} \sum_{k=0}^{i-2-j} \frac{(i-2-j)!}{(i-2-j-k)!i^{k+1}} \Bigg\{ \frac{i}{i-1-j-k} \\ \left[(\frac{E_c}{i\eta T_c \overline{P}} + \frac{P_{th}}{\overline{P}})^{i-1-j-k} - (\frac{P_{th}}{\overline{P}})^{i-1-j-k} \right] - \left[(\frac{E_c}{i\eta T_c \overline{P}} + \frac{P_{th}}{\overline{P}})^{i-2-j-k} \right. \\ \left. -(\frac{P_{th}}{\overline{P}})^{i-2-j-k} \right] \Bigg\} + \sum_{s=0}^{m-j} (-1)^{m-j-s} C_{m-j}^{s} \frac{i^s}{i-1-j-s} \Bigg\{ \frac{i}{i-j} \\ \left[(\frac{E_c}{i\eta T_c \overline{P}} + \frac{P_{th}}{\overline{P}})^{i-j} - (\frac{P_{th}}{\overline{P}})^{i-j} \right] - \left[(\frac{E_c}{i\eta T_c \overline{P}} + \frac{P_{th}}{\overline{P}})^{i-1-j} \right. \\ \left. -(\frac{P_{th}}{\overline{P}})^{i-1-j} \right] - (\frac{P_{th}}{\overline{P}})^{i-1-j-s} \frac{i}{s+1} \left[(\frac{E_c}{i\eta T_c \overline{P}} + \frac{P_{th}}{\overline{P}})^{s+1} - (\frac{P_{th}}{\overline{P}})^{s+1} \right] \\ +(\frac{P_{th}}{\overline{P}})^{i-1-j-s} \left[(\frac{E_c}{i\eta T_c \overline{P}} + \frac{P_{th}}{\overline{P}})^{s} - (\frac{P_{th}}{\overline{P}})^{s} \right] \Bigg\} \Bigg\} \\ + \frac{(K-1)E_c}{\eta T_c \overline{P}} (1-e^{-\frac{P_{th}}{\overline{P}}})^{K-2} e^{-\frac{P_{th}}{\overline{P}}} + e^{-\frac{E_c}{\overline{P}\eta T_c}-\frac{P_{th}}{\overline{P}}} (1-e^{-\frac{P_{th}}{\overline{P}}})^{K-1}, & K > 2; \\ e^{-\frac{E_c}{\overline{P}\eta T_c}-\frac{P_{th}}{\overline{P}}} (1-e^{-\frac{P_{th}}{\overline{P}}} + \frac{E_c}{\overline{P}\eta T_c} e^{-\frac{P_{th}}{\overline{P}}}), & K = 2. \end{cases} \tag{3.12}$$

It is easy to show that the probability that the sensor can be fully charged in one coherence time ($K = 1$) can be calculated as

$$\Pr[T_d = T_c] = \Pr[E_h^{(1)} \geq E_c] = e^{-\frac{E_c}{\eta T_c \overline{P}} - \frac{P_{th}}{\overline{P}}}. \tag{3.13}$$

Finally, the average number of T_c for fully charging the sensor is calculated as

$$\overline{K} = \sum_{K=1}^{\infty} K \Pr[T_d = KT_c] = \frac{e^{\frac{P_{th}}{\overline{P}}}}{\eta T_c \overline{P}} E_c + e^{\frac{P_{th}}{\overline{P}}}, \tag{3.14}$$

which is a linear function of the capacity of the sensor, as expected by intuition.

3.4.2 Packet Delay with Retransmission

The sensor node will start packet transmission after being fully charged. We again assume that for the sink to successfully decode a packet, the received SINR should be above a threshold γ_T. The packet error probability at the sink is mathematically

given by

$$P_E = \Pr[\gamma_s < \gamma_T] = \Pr\left[\frac{\frac{E_c}{T_s d_T^\lambda}||g_s||^2}{\frac{P_T}{d_I^\lambda}||h_s||^2 + \Gamma\sigma^2} < \gamma_T\right], \tag{3.15}$$

where $\frac{E_c}{T_s}$ is the sensor transmission power. The close form expression of P_E can be obtained using the PDFs of $||h_s||^2$ and $||g_s||^2$, given in (3.8), as

$$P_E = \int_0^\infty \int_0^{\frac{T_s\gamma_T d_T^\lambda(\frac{P_T y}{d_I^\lambda}+\Gamma\sigma^2)}{E_c}} f_{||h_s||^2}(x) f_{||g_s||^2}(y) dxdy = 1 - \frac{E_c e^{-\frac{\Gamma\sigma^2 T_s\gamma_T d_T^\lambda}{E_c}}}{E_c + \frac{P_T}{d_I^\lambda} T_s\gamma_T d_T^\lambda}. \tag{3.16}$$

If the received SINR at the sink is below γ_T, the sensor will repeat the energy harvesting and packet transmission until the packet is decoded correctly. Consequently, the average delay for successfully transmitting a packet to the sink can be calculated as

$$\overline{T}_{CB} = (\overline{K}T_c + T_s)\sum_{i=1}^{\infty} iP_E^{i-1}(1-P_E) = \frac{\overline{K}T_c + T_s}{1-P_E}, \tag{3.17}$$

where the term $\overline{K}T_c + T_s$ represents the average time duration for one charging and packet transmission cycle and $P_E^{i-1}(1-P_E)$ denotes the probability that the packet can be successfully delivered after ith transmission. Then by substituting (3.5) and (3.14) into (3.17), the close form expression of the overall average delay for successfully packet transmission can be given by

$$\overline{T}_{CB} = \left[\left(\frac{E_c}{\eta\overline{P}} + T_c\right)e^{\frac{P_{th}}{\overline{P}}} + T_s\right]\left(1 + \frac{P_T T_s\gamma_T d_T^\lambda}{d_I^\lambda E_c}\right)e^{\frac{\Gamma\sigma^2\gamma_T T_s d_T^\lambda}{E_c}}. \tag{3.18}$$

3.4.3 Optimal Energy Storage Capacity

Intuitively, larger energy storage capacity of the sensor will lead to longer time required for fully charging the sensor, but smaller probability for transmission failure, which will help reduce the average number of retransmission for packet delivery. Thus, we are interested in finding an optimal energy capacity of the sensor, denoted by E_{CB}^*,

to minimize $\overline{T}_{CB}$. By calculating the derivative of $\overline{T}_{CB}$ with respect to E_c and setting it to zero, we have

$$E_c^3 - \Gamma\sigma^2 T_s \gamma_T d_T^\lambda E_c^2 - T_s \gamma_T d_T^\lambda \Bigg[\eta \overline{P} (\frac{P_T}{d_I^\lambda} + \Gamma\sigma^2)(T_c + T_s e^{-\frac{P_{th}}{\overline{P}}}) + \frac{P_T \Gamma\sigma^2 T_s \gamma_T d_T^\lambda}{d_I^\lambda} \Bigg] E_c - \eta \overline{P} P_T \Gamma\sigma^2 T_s^2 \gamma_T^2 d_T^{2\lambda} (T_c + T_s e^{-\frac{P_{th}}{\overline{P}}}) \frac{P_T}{d_I^\lambda} = 0, \quad (3.19)$$

which is the homogeneous equation of E_c with order 3. The optimal energy capacity E_{CB}^* is the solution of (3.19), that satisfies $\frac{dT_p(E_c^-)}{dE_c^-} \leq 0, \frac{dT_p(E_c^+)}{dE_c^+} \geq 0$ and $E_c > 0$. We found that for most practical values of system parameters, there only exists one unique solution. One can easily find the ultimate minimum if more than one solution exists, given the simplicity of the objective function.

Since in general the packet transmission time T_s is much smaller than the channel coherence time T_c for low rate sensing application targeted here, (3.19) can be further simplified by omitting the terms involving $\mathcal{O}(T_s^2)$ as

$$E_c^2 - \Gamma\sigma^2 T_s \gamma_T d_T^\lambda E_c - \eta \overline{P} T_c T_s \gamma_T d_T^\lambda \left(\frac{P_T}{d_I^\lambda} + \Gamma\sigma^2 \right) = 0. \quad (3.20)$$

Then the close-to-optimal energy capacity to minimize the average transmission delay can be calculated as

$$E_{CB}^* \approx \frac{\Gamma\sigma^2 T_s \gamma_T d_T^\lambda + \sqrt{(\Gamma\sigma^2 T_s \gamma_T d_T^\lambda)^2 + 4\eta \overline{P} T_c T_s \gamma_T d_T^\lambda (\frac{P_T}{d_I^\lambda} + \Gamma\sigma^2)}}{2}. \quad (3.21)$$

3.4.4 Numerical Examples

In Fig. 3.5, we plot the probability mass function (PMF) of the number of coherence time needed for the sensor to harvest at least $E_c = 0.004J$ energy. The PMF obtained through monte carlo simulation are also presented. As we can see, the analytical results match the simulation result perfectly, which verifies our analytical derivation.

In Fig. 3.6, we plot the average packet transmission delay for the channel blind strategy as a function of the sensor energy storage E_c with $\gamma_T = 20dB$. It is shown that with the increase of E_c, the packet delay first quickly reduces, and then gradually increases. The reason is that, when E_c is small, the sensor can be fully charged quickly, but the sink can not decode the packet due to low received SINR. The sensor has

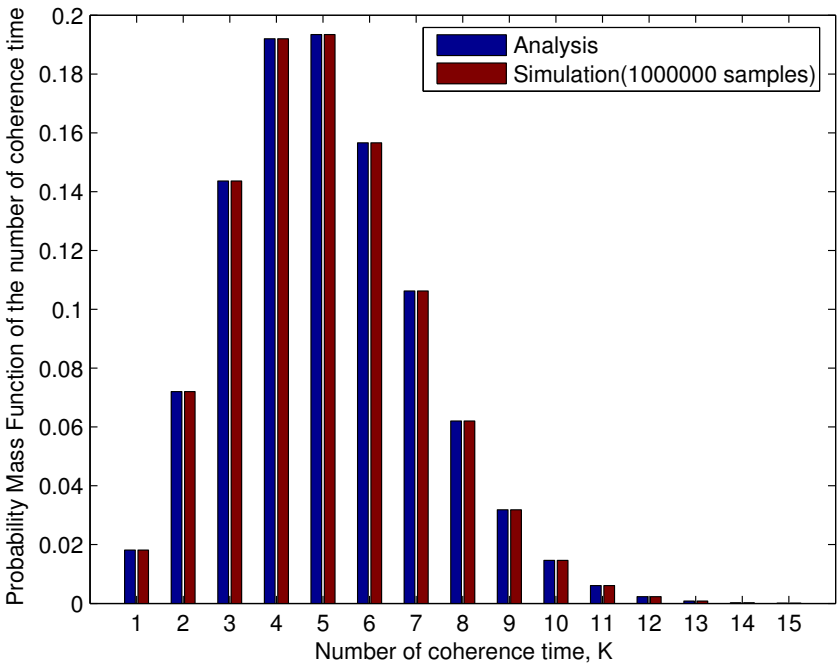

Figure 3.5: Distribution of the number of channel coherence time required for fully charging the sensor.

to retransmit the packet multiple times, leading to large average delay. When E_c increases, the delay for packet retransmission reduces as the transmission typically enjoys high SINR, but the sensor now needs more time to harvest enough energy. We also mark the approximated and exact values of the optimal energy capacity E^*_{CB}. We observe that the near-to-optimal solution achieves almost the same average delay performance as the exact optimal energy capacity value.

3.5 Channel-Aware Transmission Strategy for Delay Insensitive Traffic

In this section, we consider an alternative transmission strategy for delay insensitive traffic and evaluate its delay performance. Note that with the channel blind strategy, the sensor will transmit its packet immediately after harvesting enough energy, which may not be successful due to poor signal channel or strong interference in the coming channel coherence time, and thus leads to the waste of harvested RF energy. To better utilize the harvested energy, we consider a channel-aware transmission strategy

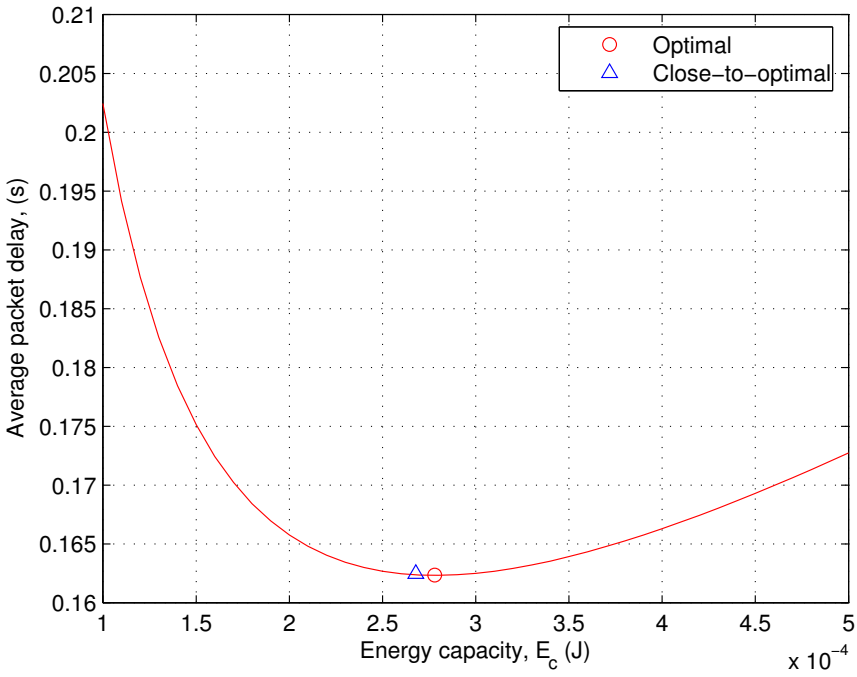

Figure 3.6: Average packet delay versus energy capacity E_c for channel blind strategy for delay insensitive traffic.

in this section. Specifically, we again assume that the sensor will harvest RF energy from the BS until being fully charged. After that, instead of transmitting its packet immediately, the sensor will decide whether to transmit or not according to the instantaneous received SINR estimation at the sink. A packet will be transmitted only if the experienced SINR at the sink is larger than γ_T, which will lead to successful delivery. If the SINR at the sink is below γ_T, then the sensor will hold its transmission for future channel coherence time until the SINR is above γ_T. We assume the sink can precisely estimate the signal and interference channel, and feed back the SINR to the sensor at the beginning of each channel coherence time.

We again focus on the average packet delay performance for packet delivery and would like to quantify the benefit, if any, that the channel information can bring in terms of delay reduction. Note that total packet transmission delay becomes the sum of the sensor changing time, the waiting time for packet transmission, and the packet transmission time T_s.

3.5.1 Delay Analysis

We first derive the statistics of the waiting time for packet transmission, i.e. the number of channel coherence time T_c that the sensor needs to wait before the SINR at the sink is larger than γ_T and packet transmission can start. Let $\Pr[T_w = MT_c]$ denote the probability that the sensor needs to wait M channel coherence time before packet transmission, which is equal to the probability that the SINR at the sink during each of the first M coherence time is less than γ_T, and that during the $M+1$th coherence time larger than γ_T. Therefore, we can mathematically calculate $\Pr[T_w = MT_c]$ as

$$\Pr[T_w = MT_c] = P_E^M(1-P_E) = \left(1 - \frac{E_c e^{-\frac{\Gamma\sigma^2 T_s \gamma_T d_T^\lambda}{E_c}}}{E_c + \frac{P_T}{d_I^\lambda} T_s \gamma_T d_T^\lambda}\right)^M \left(\frac{E_c e^{-\frac{\Gamma\sigma^2 T_s \gamma_T d_T^\lambda}{E_c}}}{E_c + \frac{P_T}{d_I^\lambda} T_s \gamma_T d_T^\lambda}\right), \quad (3.22)$$

where P_E denotes the probability that the instantaneous received SINR at the sink is below γ_T, which has been calculated in (3.16).

The distribution of the total delay for packet transmission can be given by

$$\Pr[T_{CA} = LT_c + T_s] = \sum_{K=1}^{L} \Pr[T_d = KT_c] \Pr[T_w = (L-K)T_c], \quad (3.23)$$

where $\Pr[T_d = KT_c]$ denotes the probability that K channel coherence time is needed

to fully charge the sensor, which has been derived in (3.12) and (3.13). After substituting (3.12), (3.13) and (3.22) into (3.23) and some manipulations, the close-form expression for the probability mass function (PMF) of the total packet transmission delay with channel-aware transmission strategy can be calculated as

$$
\begin{aligned}
&\Pr[T_{CA} = LT_c + T_s] \quad = \\
&\begin{cases}
e^{-\frac{E_c}{\overline{P}\eta T_c}-\frac{P_{th}}{\overline{P}}}\left(\frac{E_c e^{-\frac{\Gamma\sigma^2 T_s\gamma_T d_T^\lambda}{E_c}}}{E_c+\frac{P_T}{d_I^\lambda}T_s\gamma_T d_T^\lambda}\right), & L=1;\\
e^{-\frac{E_c}{\overline{P}\eta T_c}-\frac{P_{th}}{\overline{P}}}\left(1-e^{-\frac{P_{th}}{\overline{P}}}+\frac{E_c}{\overline{P}\eta T_c}e^{-\frac{P_{th}}{\overline{P}}}\right)\left(\frac{E_c e^{-\frac{\Gamma\sigma^2 T_s\gamma_T d_T^\lambda}{E_c}}}{E_c+\frac{P_T}{d_I^\lambda}T_s\gamma_T d_T^\lambda}\right)\\
+e^{-\frac{E_c}{\overline{P}\eta T_c}-\frac{P_{th}}{\overline{P}}}\left(1-\frac{E_c e^{-\frac{\Gamma\sigma^2 T_s\gamma_T d_T^\lambda}{E_c}}}{E_c+\frac{P_T}{d_I^\lambda}T_s\gamma_T d_T^\lambda}\right)\left(\frac{E_c e^{-\frac{\Gamma\sigma^2 T_s\gamma_T d_T^\lambda}{E_c}}}{E_c+\frac{P_T}{d_I^\lambda}T_s\gamma_T d_T^\lambda}\right), & L=2;\\
\sum_{K=3}^{L}\Bigg\{e^{-\frac{E_c}{\overline{P}\eta T_c}-\frac{P_{th}}{\overline{P}}}\sum_{i=2}^{K-1}\frac{(K-1)!(1-e^{-\frac{P_{th}}{\overline{P}}})^{K-1-i}e^{-\frac{iP_{th}}{\overline{P}}}}{(i-1)!(i-2)!(K-1-i)!}\\
\sum_{m=0}^{i-2}(1-i)^{i-2-m}C_{i-2}^{m}\sum_{j=0}^{m}\frac{m!}{(m-j)!}\Bigg\{(i-1)^{m-j}\sum_{k=0}^{i-2-j}\\
\frac{(i-2-j)!}{(i-2-j-k)!i^{k+1}}\Bigg\{\frac{i}{i-1-j-k}\left[\left(\frac{E_c}{i\eta T_c\overline{P}}+\frac{P_{th}}{\overline{P}}\right)^{i-1-j-k}-\left(\frac{P_{th}}{\overline{P}}\right)^{i-1-j-k}\right]\\
-\left[\left(\frac{E_c}{i\eta T_c\overline{P}}+\frac{P_{th}}{\overline{P}}\right)^{i-2-j-k}-\left(\frac{P_{th}}{\overline{P}}\right)^{i-2-j-k}\right]\Bigg\}\\
+\sum_{s=0}^{m-j}(-1)^{m-j-s}C_{m-j}^{s}\frac{i^s}{i-1-j-s}\Bigg\{\frac{i}{i-j}\left[\left(\frac{E_c}{i\eta T_c\overline{P}}+\frac{P_{th}}{\overline{P}}\right)^{i-j}-\left(\frac{P_{th}}{\overline{P}}\right)^{i-j}\right]\\
-\left[\left(\frac{E_c}{i\eta T_c\overline{P}}+\frac{P_{th}}{\overline{P}}\right)^{i-1-j}-\left(\frac{P_{th}}{\overline{P}}\right)^{i-1-j}\right]\\
-\left(\frac{P_{th}}{\overline{P}}\right)^{i-1-j-s}\frac{i}{s+1}\left[\left(\frac{E_c}{i\eta T_c\overline{P}}+\frac{P_{th}}{\overline{P}}\right)^{s+1}-\left(\frac{P_{th}}{\overline{P}}\right)^{s+1}\right]\\
+\left(\frac{P_{th}}{\overline{P}}\right)^{i-1-j-s}\left[\left(\frac{E_c}{i\eta T_c\overline{P}}+\frac{P_{th}}{\overline{P}}\right)^{s}-\left(\frac{P_{th}}{\overline{P}}\right)^{s}\right]\Bigg\}\Bigg\}\\
+\frac{(K-1)E_c}{\eta T_c\overline{P}}\left(1-e^{-\frac{P_{th}}{\overline{P}}}\right)^{K-2}e^{-\frac{P_{th}}{\overline{P}}}+\left(1-e^{-\frac{P_{th}}{\overline{P}}}\right)^{K-1}\Bigg\}\\
\left(1-\frac{E_c e^{-\frac{\Gamma\sigma^2 T_s\gamma_T d_T^\lambda}{E_c}}}{E_c+\frac{P_T}{d_I^\lambda}T_s\gamma_T d_T^\lambda}\right)^{L-K}\left(\frac{E_c e^{-\frac{\Gamma\sigma^2 T_s\gamma_T d_T^\lambda}{E_c}}}{E_c+\frac{P_T}{d_I^\lambda}T_s\gamma_T d_T^\lambda}\right)\\
+e^{-\frac{E_c}{\overline{P}\eta T_c}-\frac{P_{th}}{\overline{P}}}\left(1-e^{-\frac{P_{th}}{\overline{P}}}+\frac{E_c}{\overline{P}\eta T_c}e^{-\frac{P_{th}}{\overline{P}}}\right)\\
\left(1-\frac{E_c e^{-\frac{\Gamma\sigma^2 T_s\gamma_T d_T^\lambda}{E_c}}}{E_c+\frac{P_T}{d_I^\lambda}T_s\gamma_T d_T^\lambda}\right)^{L-2}\left(\frac{E_c e^{-\frac{\Gamma\sigma^2 T_s\gamma_T d_T^\lambda}{E_c}}}{E_c+\frac{P_T}{d_I^\lambda}T_s\gamma_T d_T^\lambda}\right)\\
+e^{-\frac{E_c}{\overline{P}\eta T_c}-\frac{P_{th}}{\overline{P}}}\left(1-\frac{E_c e^{-\frac{\Gamma\sigma^2 T_s\gamma_T d_T^\lambda}{E_c}}}{E_c+\frac{P_T}{d_I^\lambda}T_s\gamma_T d_T^\lambda}\right)^{L-1}\left(\frac{E_c e^{-\frac{\Gamma\sigma^2 T_s\gamma_T d_T^\lambda}{E_c}}}{E_c+\frac{P_T}{d_I^\lambda}T_s\gamma_T d_T^\lambda}\right), & L>2.
\end{cases}
\end{aligned}
\tag{3.24}
$$

With the PMF of T_{CA}, we can readily calculate the average packet transmission delay, $\overline{T}_{CA}$. Alternatively, we can first calculate the average number of T_c that the sensor

needs to wait for packet transmission using (3.22) as

$$\overline{M} = \sum_{M=0}^{\infty} M \Pr[T_w = MT_c] = \frac{P_E}{1-P_E} = \left(1 + \frac{P_T T_s \gamma_T d_T^{\lambda}}{E_c d_I^{\lambda}}\right) e^{\frac{\sigma^2 \gamma_T T_s \Gamma d_T^{\lambda}}{E_c}} - 1. \quad (3.25)$$

Finally, the average delay for successfully transmitting a packet to the sink can be calculated, by combining the results in (3.14) and (3.25), as

$$\begin{aligned} \overline{T}_{CA} &= (\overline{K} + \overline{M})T_c + T_s \\ &= \left[\frac{e^{\frac{P_{th}}{\overline{P}}}}{\overline{P}\eta T_c} E_c + e^{\frac{P_{th}}{\overline{P}}} + \left(1 + \frac{P_T T_s \gamma_T d_T^{\lambda}}{E_c d_I^{\lambda}}\right) e^{\frac{\Gamma\sigma^2 T_s \gamma_T d_T^{\lambda}}{E_c}} - 1\right] T_c + T_s. \quad (3.26) \end{aligned}$$

3.5.2 Optimal Energy Storage Capacity

Intuitively, larger energy storage capacity at the sensor E_c will lead to longer charging time, but smaller waiting time until the received SINR at the sink becomes larger than γ_T. Thus, we expect there is also an optimal value of sensor energy capacity to minimize $\overline{T}_{CA}$. By calculating the derivative of $\overline{T}_{CA}$ with respect to E_c and setting it to zero, we have equation

$$E_c^3 - \eta \overline{P} T_c \left[T_s \gamma_T d_T^{\lambda} \left(\frac{P_T}{d_I^{\lambda}} + \Gamma\sigma^2\right) E_c + \frac{\Gamma\sigma^2 P_T (T_s \gamma_T d_T^{\lambda})^2}{d_I^{\lambda}}\right] e^{\frac{\sigma^2 \gamma_T T_s \Gamma d_T^{\lambda}}{E_c} - \frac{P_{th}}{\overline{P}}} = 0. \quad (3.27)$$

To precede further, we apply Taylor series expansion to the exponential term around T_s, which is typically very small, as

$$e^{\frac{\Gamma\sigma^2 \gamma_T d_T^{\lambda}}{E_c} T_s} = 1 + \frac{\Gamma\sigma^2 \gamma_T d_T^{\lambda}}{E_c} T_s + \mathcal{O}(T_s^2). \quad (3.28)$$

By substituting (3.28) into (3.27) and omitting the terms involving $\mathcal{O}(T_s^2)$, we have

$$E_c^2 - \eta \overline{P} T_c T_s \gamma_T d_T^{\lambda} \left(\frac{P_T}{d_I^{\lambda}} + \Gamma\sigma^2\right) e^{-\frac{P_{th}}{\overline{P}}} = 0. \quad (3.29)$$

Then the close-to-optimal energy capacity to minimize the average transmission delay, denoted by E_{CA}^*, can be calculated as

$$E_{CA}^* \approx \sqrt{\eta \overline{P} T_c T_s \gamma_T d_T^{\lambda} \left(\frac{P_T}{d_I^{\lambda}} + \Gamma\sigma^2\right) e^{-\frac{P_{th}}{\overline{P}}}}. \quad (3.30)$$

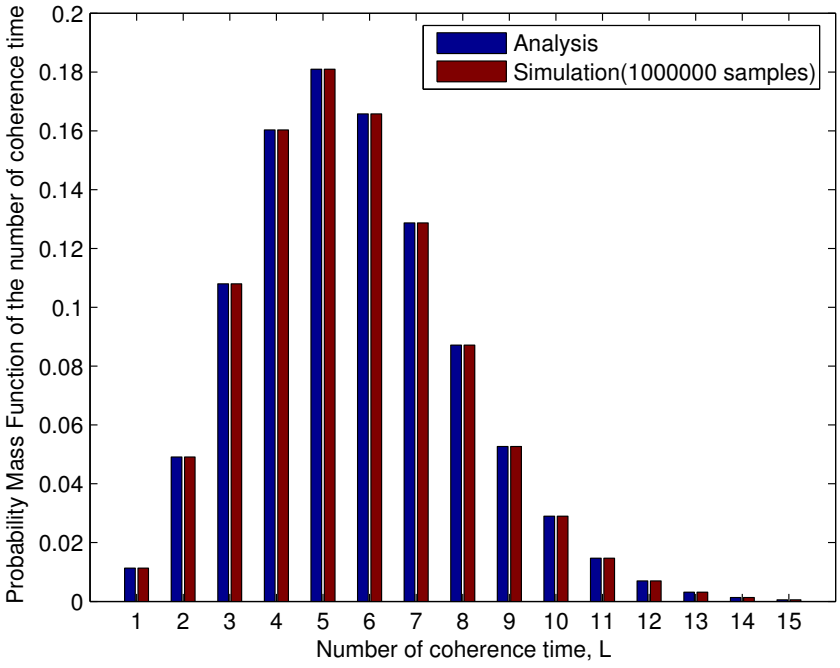

Figure 3.7: Distribution of the number of channel coherence time needed for packet transmission.

3.5.3 Numerical Examples

In Fig. 3.7, we plot the PMF of the number of coherence time needed to transmit a packet with the channel-aware transmission strategy for $E_c = 0.004J$ and $\gamma_T = 20dB$. The Monte Carlo simulation results are also presented. As we can see, the analytical result matches the simulation result perfectly, which validates our analytical approach.

In Fig. 3.8, we plot the average packet delay as a function of the energy storage capacity of the sensor for both channel aware and channel blind transmission strategies. It is observed that with the increase of E_c, the packet delay for the channel aware strategy first quickly reduces, and then gradually increases in an close-to-linear fashion. The reason is that, when E_c is small, the sensor can be fully charged quickly, but has to wait for a long time until the received SINR at the sink is larger than γ_T, leading to large average total delay. When E_c increases, the delay for waiting for packet transmission reduces, but the sensor needs more time to get fully charged. We mark the approximated values of the optimal energy capacity E^*_{CA}. The near-to-optimal solution achieves almost the same average delay performance as the exact value of optimal energy capacity. Fig. 3.8 also shows that the average packet delay of

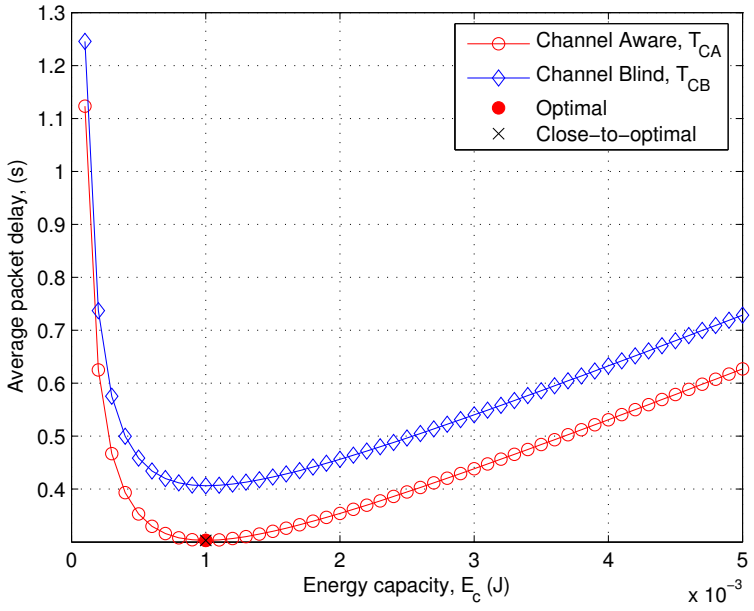

Figure 3.8: Average packet delay of two transmission strategies for delay insensitive traffic.

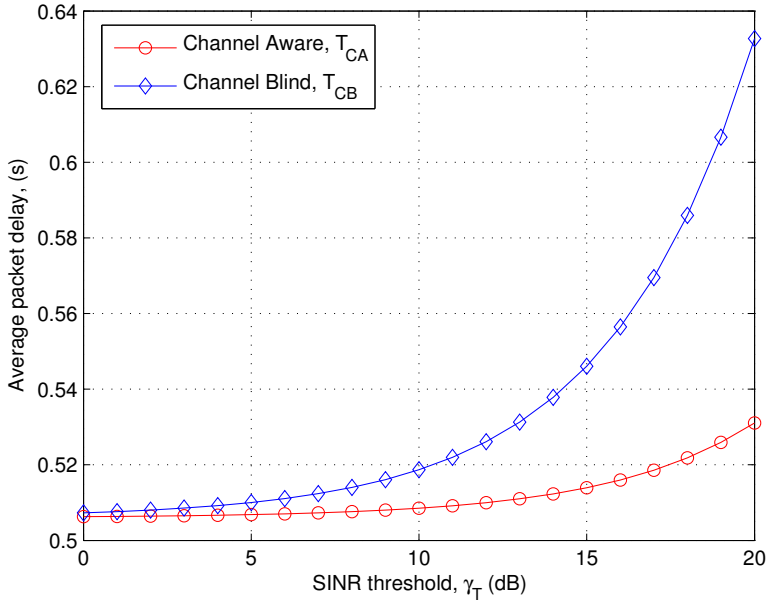

Figure 3.9: Average packet delay versus packet loss threshold γ_T for two transmission strategies for delay insensitive traffic.

the channel aware strategy is much smaller than that of the channel blind strategy. The instantaneous SINR obtained at the beginning of each coherence time not only helps avoid wasted packet transmission and the associated recharging, but also reduce the average total packet transmission delay. This observation is further confirmed in Fig. 3.9, where we plot the average packet delay as a function of the SINR threshold γ_T for both channel aware and channel blind strategies. It is observed that with the increase of γ_T, the packet transmission delay for both strategies increase quickly, and the packet delay for the channel blind strategy grows faster than that for the channel aware strategy.

3.6 Concluding Remarks

In this Chapter, we investigated the packet transmission performance of wireless sensor nodes powered by harvesting RF energy from existing wireless systems. Different from previous works, we considered the packet effect of fading channel variation on both energy harvesting and information transmission. For energy harvesting stage, we investigated and obtained the close-form expression of the distribution functions of harvested energy over multiple channel coherence time. The distribution of harvested energy is calculated based on a practical operation model for energy harvesting, considering harvesting sensitivity, harvesting efficiency and energy capacity. For the packet transmission stage, we took into account the effects of interference from existing wireless system. We accurately quantified the transmission performance of the proposed implementation for sensor applications with low traffic intensity. We also investigated the optimization of energy capacity of the sensor to minimize the average delay for delay insensitive traffic. The analytical results will greatly facilitate the practical design of sensor network powered by RF energy harvesting for the appropriate target sensing applications.

3.7 Appendix: Distribution of Harvested Energy over N Channel Coherence Time

We first consider the one coherence time case, i.e. $N = 1$. The CDF of the harvested energy can be simply represented as

$$F_{E_h^{(1)}}(x) = \Pr[E_h^{(1)} < x] = \Pr[E_1 < x], \quad x \leq E_c. \tag{3.31}$$

After substituing (3.3) into (3.31) and some manipulation, we have

$$F_{E_h^{(1)}}(x) = 1 - e^{-\frac{x}{\eta T_c \overline{P}} - \frac{P_{th}}{\overline{P}}}, \quad x \leq E_c. \tag{3.32}$$

For the multiple channel coherence time case, i.e. $N > 1$, we denote the number of channel coherence time, in which the sensor can harvest energy, by N_a. According to the total probability theorem, the CDF of the harvested energy is shown as

$$F_{E_h^{(N)}}(x) = \Pr[E_h^{(N)} < x] = \sum_{i=0}^{N} \Pr[\sum_{n=1}^{N} E_n < x, N_a = i]. \tag{3.33}$$

When the ith largest received power is larger than P_{th} and the $(i+1)$th largest one is lower than P_{th}, the number of coherence time that the sensor can harvest energy is $N_a = i$. We denote the ordered version of N i.i.d. random variables α_n as $\alpha_{1:N} \geq \alpha_{2:N} \geq \cdots \geq \alpha_{N:N}$, and the sum of the $i-1$ largest variables as $\beta_i = \sum_{j=1}^{i-1} \alpha_{j:N}$. We can show that $N_a = i$ if and only if $\alpha_{i:N} \geq \frac{\Gamma d_H^{\lambda} P_{th}}{P_T}$ and $\alpha_{i+1:N} < \frac{\Gamma d_H^{\lambda} P_{th}}{P_T}$. Therefore,

$F_{E_h}(x)$ can be calculated as

$$\begin{aligned} F_{E_h^{(N)}}(x) &= \sum_{i=2}^{N-1} \Pr[\beta_i + \alpha_{i:N} < \frac{x}{\eta T_c \overline{P}} + \frac{iP_{th}}{\overline{P}}, \alpha_{i:N} \geq \frac{P_{th}}{\overline{P}}, \alpha_{i+1:N} < \frac{P_{th}}{\overline{P}}] \quad (3.34) \\ &\quad + \Pr[\alpha_{1:N} < \frac{P_{th}}{\overline{P}}] + \Pr[\frac{P_{th}}{\overline{P}} \leq \alpha_{1:N} < \frac{x}{\eta T_c \overline{P}} + \frac{P_{th}}{\overline{P}}, \alpha_{2:N} < \frac{P_{th}}{\overline{P}}] \\ &\quad + \Pr[\beta_N + \alpha_{N:N} < \frac{x}{\eta T_c \overline{P}} + \frac{NP_{th}}{\overline{P}}, \alpha_{N:N} \geq \frac{P_{th}}{\overline{P}}] \\ &= \sum_{i=2}^{N-1} \int_{\frac{P_{th}}{\overline{P}}}^{\frac{x}{i\eta T_c \overline{P}} + \frac{P_{th}}{\overline{P}}} \int_{(i-1)y}^{\frac{x}{\eta T_c \overline{P}} + \frac{iP_{th}}{\overline{P}} - y} \int_0^{\frac{P_{th}}{\overline{P}}} f_{\beta_i, \alpha_{i:N}, \alpha_{i+1:N}}(t, y, z) dt dy dz \\ &\quad + \int_0^{\frac{P_{th}}{\overline{P}}} f_{\alpha_{1:N}}(t) dt + \int_0^{\frac{P_{th}}{\overline{P}}} \int_{\frac{P_{th}}{\overline{P}}}^{\frac{x}{\eta T_c \overline{P}} + \frac{P_{th}}{\overline{P}}} f_{\alpha_{1:N}, \alpha_{2:N}}(t, y) dt dy \\ &\quad + \int_{\frac{P_{th}}{\overline{P}}}^{\frac{x}{N\eta T_c \overline{P}} + \frac{P_{th}}{\overline{P}}} \int_{(N-1)y}^{\frac{x}{\eta T_c \overline{P}} + \frac{NP_{th}}{\overline{P}} - y} f_{\beta_N, \alpha_{N:N}}(t, y) dt dy, \end{aligned}$$

where $f_{\alpha_{1:N}}(x, y)$, $f_{\alpha_{1:N}, \alpha_{2:N}}(x, y)$, $f_{\beta_N, \alpha_{N:N}}(x, y)$, and $f_{\beta_i, \alpha_{i:N}, \alpha_{i+1:N}}(x, y, z)$ are the marginal and joint PDFs of $\alpha_{i:N}$ and β_i. In particular, their closed-form expression for Rayleigh fading environment under consideration can be obtained as [29]

$$f_{\alpha_{1:N}}(x) = Ne^{-x}(1 - e^{-x})^{N-1}, \quad (3.35)$$

$$f_{\alpha_{1:N}, \alpha_{2:N}}(x, y) = \frac{N!}{(N-2)!} e^{-x-y}(1 - e^{-y})^{N-2}, \quad (3.36)$$

$$f_{\beta_N, \alpha_{N:N}}(x, y) = \frac{N}{(N-2)!}[x - (N-1)y]^{N-2} e^{-x-y}, \quad x \geq (N-1)y, \quad (3.37)$$

$$f_{\beta_i, \alpha_{i:N}, \alpha_{i+1:N}}(x, y, z) = \frac{N! e^{-x-y-z}(1 - e^{-z})^{N-i-1}[x - (i-1)y]^{i-2}}{(i-1)!(i-2)!(N-i-1)!}, \quad \frac{x}{i-1} > y > z. \quad (3.38)$$

By properly substituting (3.35), (3.36), (3.37) and (3.38) into (3.34) and carrying out integration, the close form expression of the CDF of harvested energy over N

coherence time is obtained as

$$
\begin{aligned}
F_{E_h^{(N)}}(x) \;=\; & \\
& \begin{cases}
\sum_{i=2}^{N} \frac{N!(1-e^{-\frac{P_{th}}{\overline{P}}})^{N-i}e^{-\frac{iP_{th}}{\overline{P}}}}{(i-1)!(i-2)!(N-i)!} \sum_{m=0}^{i-2}(1-i)^{i-2-m}C_{i-2}^{m}\sum_{j=0}^{m}\frac{m!}{(m-j)!} \\
\Big\{(i-1)^{m-j}\sum_{k=0}^{i-2-j}\frac{(i-2-j)!}{(i-2-j-k)!i^{k+1}}\Big[\big(\frac{P_{th}}{\overline{P}}\big)^{i-2-j-k} \\
-e^{-\frac{x}{\eta T_c\overline{P}}}\big(\frac{x}{i\eta T_c\overline{P}}+\frac{P_{th}}{\overline{P}}\big)^{i-2-j-k}\Big] - e^{-\frac{x}{\eta T_c\overline{P}}}\sum_{s=0}^{m-j}(-1)^{m-j-s}C_{m-j}^{s} \\
\big(\frac{x}{\eta T_c\overline{P}}+\frac{iP_{th}}{\overline{P}}\big)^{s}\frac{\big(\frac{x}{i\eta T_c\overline{P}}+\frac{P_{th}}{\overline{P}}\big)^{i-1-j-s}-\big(\frac{P_{th}}{\overline{P}}\big)^{i-1-j-s}}{i-1-j-s}\Big\} + (1-e^{-\frac{P_{th}}{\overline{P}}})^{N} \\
+N(1-e^{-\frac{P_{th}}{\overline{P}}})^{N-1}(e^{-\frac{P_{th}}{\overline{P}}}-e^{-\frac{x}{\eta T_c\overline{P}}-\frac{P_{th}}{\overline{P}}}), & x \le E_c; \\
1, & x > E_c.
\end{cases}
\end{aligned}
\tag{3.39}
$$

After taking derivative with respect to x, the PDF of $E_h^{(N)}$ is derived and given in (3.10). Note that the PDF involves two impulse function at 0 and E_c due to the capacity constraints.

Chapter 4

RF Energy Harvesting with Cooperative Beam Selection for Wireless Sensors

4.1 Introduction

The secondary transmiter can serve as both data source for its own users and RF energy source for RF-energy-powered sensor nodes. In [32], the authors investigate simultaneous wireless transmission and energy harvesting by designing optimal beamforming vector and power splitting ratio. It is shown in [25] that with channel information at the energy source node, multi-antenna transmission can help increase the amount of harvested energy at the energy receiving node. Inspired by [25], we consider a practical cooperative charging scenario in this paper, where an existing multiuser MIMO system helps the energy harvesting of a RF-energy-powered sensor node, while simultaneously serving its own users. We adopt random unitary beamforming (RUB) as the transmission scheme for multiuser MIMO systems, which requires very low feedback load, and has been incorporated in several wireless standards [33, 34]. We propose a RUB-based cooperative beam selection scheme, where the base station (BS) of the existing system selects the best beams for transmission, while trying to satisfy energy harvesting requirement of the sensor, i.e. the harvested energy over each coherence time is above a predefined energy threshold. Specifically, for the single sensor case, the BS of the MISO system selects the best beam for transmission. The number of usable beams that the BS can select from to serve its user is reduced. We

derive the closed-form statistical distribution of the amount of energy that can be harvested at the sensor, and throughput of the existing MISO system. For the multiple sensors case, the BS of the multiuser MIMO system selects a maximal number of active beams for transmission, while trying to satisfy energy harvesting requirement. With a constant total transmission power, the BS can enhance energy harvesting at the sensor by concentrating the transmission power on selected beams. Meanwhile, the number of users that the BS can serve simultaneously is reduced. To evaluate the performance tradeoff between the average harvested energy at the sensor and the existing multiuser MIMO system, we derive the closed-form statistical distribution of the amount of energy that can be harvested , as well as the sum-rate of existing MIMO system with the proposed cooperative RF energy harvesting scheme. These analytical results will help determine the optimal energy threshold value that can satisfy requirements of certain sensing applications, while considering the negative effect on the multiuser MIMO system.

4.2 System and Channel Model

4.2.1 System Model

We consider a single-antenna wireless sensor node deployed in the coverage area of an existing RUB-based multiuser MIMO system, which could be cellular or WiFi systems. The sensor [1] can harvest RF energy from the transmitted signal of the multiuser MIMO system, and use it as its sole energy source, as illustrated in Fig. 4.1. The multiuser MIMO system consists of single BS with M antennas and K single-antenna users. The BS can serve up to M selected users simultaneously using random orthonormal beams generated from an isotropic distribution. Let $\mathcal{W} = [\mathbf{w}_1, \mathbf{w}_2, \ldots, \mathbf{w}_M]^T$ denote the set of beam vectors, assumed to be known to both the BS and its users. The transmitted signal vector from M antennas over one symbol period can be written, assuming m beams are active, as $\mathbf{x} = \sum_{j=1}^{m} \sqrt{\frac{P_T}{m}} \mathbf{w}_j s_j$, where s_j denotes the information symbol for the jth selected user. Here, we assume that the transmission power P_T is constant and equally allocated to different active beams.

[1] The sensor can also be a special user of multiuser MIMO system.

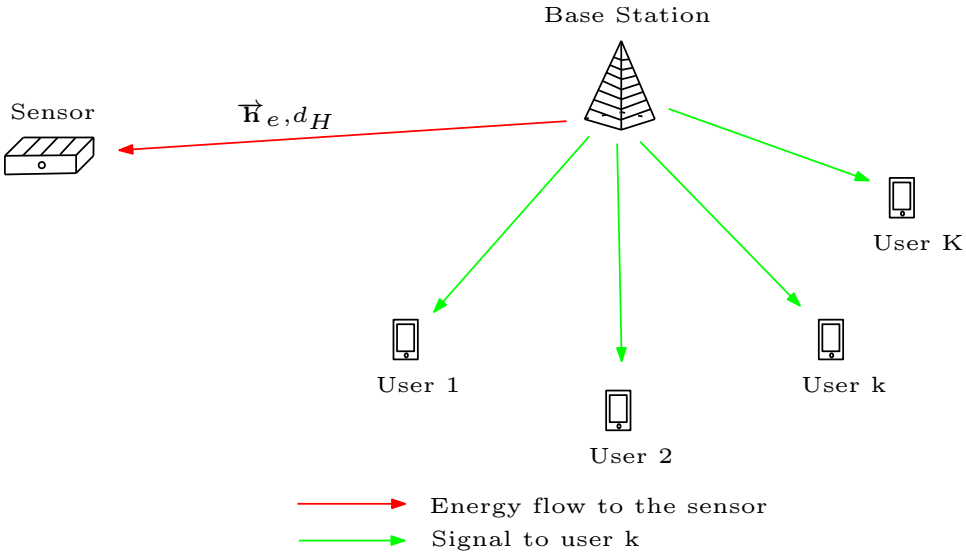

Figure 4.1: System model for RUB-based cooperative RF energy harvesting.

4.2.2 Channel Model

We adopt a log-distance path loss plus Rayleigh block slow fading channel model for the operating environment while ignoring the shadowing effect [30]. In particular, the channel gain between the BS and the sensor remains constant over one channel coherence time, denoted by T_c, and changes to an independent value afterward. Let $\mathbf{h}_e = [h_{e_1}, h_{e_2}, \ldots, h_{e_M}]^T$ denote the fading channel gain vector from the BS to the sensor, where $h_{e_m} \in \mathcal{CN}(0,1)$. Then the harvested energy at the sensor from the ith beam, when m beams are active, can be given by

$$E_i = \left(\frac{\eta T_c}{\Gamma d_H^{\lambda}}\right)\left(\frac{P_T}{m}\right)|\mathbf{h}_e^T \mathbf{w}_i|^2, \quad i = 1, 2, \ldots, m, \tag{4.1}$$

where d_H is the distance from BS to the sensor, η is the energy harvesting efficiency, λ is the path loss exponent, ranging from 2 to 5, and Γ is a constant parameter of the log-distance model. Specifically, $\Gamma = \frac{PL(d_0)}{d_0^{\lambda}}$, where d_0 is a reference distance in the antenna far field, and $PL(d_0)$ is linear path loss at distance d_0, depending on the propagation environment. For notational conciseness, we use α_m to denote the amplitude square of the projection of $\mathbf{h}_e$ onto $\mathbf{w}_m$, i.e. $\alpha_m = |\mathbf{h}_e^T \mathbf{w}_m|^2$, whose probability density function (PDF) for Rayleigh fading channel under consideration is given by

$$f_{\alpha_m}(x) = e^{-x}. \tag{4.2}$$

4.3 RUB-based Cooperative Energy Harvesting for Single Sensor

4.3.1 Mode of Cooperation

With the proposed cooperative energy harvesting scheme, the BS will select the best beam to serve the user, while ensuring that the harvested energy at the sensor node during each coherence time is above a predefined energy threshold E_{th}.

At the beginning of each channel coherence time, the BS first estimates the channel vector from the BS to the sensor. The BS then calculates and ranks the projection amplitude square α_m for each beam, the order version of which is denoted by $\alpha_{m:M}$, where $\alpha_{1:M} \geq \alpha_{2:M} \geq \cdots \geq \alpha_{M:M}$. After that, the BS calculates the amount of RF

energy that the sensor can harvest when the BS uses each beam, corresponding to $\alpha_{1:M}$ to $\alpha_{M:M}$. Specifically, the harvested energy denoted by $E_{i:M}$, when the ith best beam are used for transmission, is given by

$$E_{i:M} = \left(\frac{\eta P_T T_c}{\Gamma d_H^{\lambda}}\right)\alpha_{i:M}, \quad i = 1, 2, \ldots, M. \tag{4.3}$$

If the harvested energy from the ith best beam is larger than the predefined energy threshold E_{th}, whereas the harvested energy from the $(i+1)$th best beam is less than E_{th}, i.e. $E_{i:M} \geq E_{th}$, and $E_{i+1:M} < E_{th}$, then the BS selects one beam from best i beams, corresponding to $\alpha_{1:M}$ to $\alpha_{i:M}$, to serve its user. It is worth noting that the amount of harvested energy at the sensor may be smaller than E_{th} even when the BS allocates the best beam j^* corresponding to $\alpha_{1:M}$, i.e. $j^* = \arg\max_j(|\mathbf{h}_e^T \mathbf{w}_j|^2)$. In this case, the BS will still use beam j^* with transmission power P_T to charge the sensor as well as serve its user.

4.3.2 Distribution of the Number of Usable Beams

In the following, we derive the probability mass function of the number of usable beams M_a ($1 \leq M_a \leq M$) that the BS can use, which will be applied to the throughput analysis for the MISO system.

According to our proposed cooperative beam selection scheme, the number of usable beams M_a is equal to m ($1 < m < M$) if and only if $E_{m:M} \geq E_{th}$, and $E_{m+1:M} < E_{th}$. Furthermore, the number of usable beams M_a is equal to 1 if the energy threshold can not be satisfied with all transmission power P_T allocated to the best beam, i.e., $E_{1:M} < E_{th}$, or if only the best beam can lead to harvest energy larger than E_{th}, i.e., $E_{1:M} \geq E_{th}$, and $E_{2:M} < E_{th}$. The number of usable beams M_a is equal to M if the harvested energy is larger than E_{th} with P_T allocated to the worst beam, i.e., $E_{M:M} \geq E_{th}$. Therefore, the probability that M_a beams are usable can be given by

$$\Pr[M_a = i] = \begin{cases} \Pr[E_{1:M} < E_{th}] + \Pr[E_{1:M} \geq E_{th}, E_{2:M} < E_{th}], & i = 1, \\ \Pr[E_{i:M} \geq E_{th}, E_{i+1:M} < E_{th}], & 1 < i < M, \\ \Pr[E_{M:M} \geq E_{th}], & i = M. \end{cases} \tag{4.4}$$

After substituting (4.3) into (4.4) and some manipulations, (4.4) can be rewritten as

$$\Pr[M_a = i] = \begin{cases} \int_0^{\frac{E_{th}}{\Lambda}} f_{\alpha_{1:M}}(x)dx + \int_0^{\frac{E_{th}}{\Lambda}} \int_{\frac{E_{th}}{\Lambda}}^{\infty} f_{\alpha_{1:M},\alpha_{2:M}}(x,y)dxdy, & i = 1, \\ \int_0^{\frac{E_{th}}{\Lambda}} \int_{\frac{E_{th}}{\Lambda}}^{\infty} f_{\alpha_{i:M},\alpha_{i+1:M}}(x,y)dxdy, & 1 < i < M, \\ \int_{\frac{E_{th}}{\Lambda}}^{\infty} f_{\alpha_{M:M}}(x)dx, & i = M, \end{cases} \tag{4.5}$$

where Λ is a constant parameter equal to $\frac{\eta P_T T_c}{\Gamma d_H^{\lambda}}$, the PDF of $\alpha_{1:M}$, and $\alpha_{M:M}$, and the joint PDF of $\alpha_{i:M}$ and $\alpha_{i+1:M}$, can be given by [29]

$$f_{\alpha_{1:M}}(x) = M(1 - e^{-x})^{M-1}e^{-x}, \tag{4.6}$$

$$f_{\alpha_{i:M},\alpha_{i+1:M}}(x,y) = \frac{M!e^{-ix-y}(1-e^{-y})^{M-i-1}}{(i-1)!(M-i-1)!}, \ x > y, \tag{4.7}$$

and

$$f_{\alpha_{M:M}}(x) = Me^{-Mx}, \tag{4.8}$$

respectively. By substituting (4.6), (4.7), and (4.8) into (4.5) and carrying out integration, the close form expression of $\Pr[M_a = i]$ is calculated as

$$\Pr[M_a = i] = \begin{cases} M\sum_{j=0}^{M-1}\binom{M-1}{j}\frac{(-1)^j}{j+1}(1 - e^{-(j+1)\frac{E_{th}}{\Lambda}}) \\ +\frac{M!e^{-\frac{E_{th}}{\Lambda}}}{(M-2)!}\sum_{j=0}^{M-2}\binom{M-2}{j}\frac{(-1)^j}{j+1}(1 - e^{-(j+1)\frac{E_{th}}{\Lambda}}), & i = 1, \\ \frac{M!e^{-i\frac{E_{th}}{\Lambda}}}{i!(M-i-1)!}\sum_{j=0}^{M-i-1}(-1)^j\binom{M-i-1}{j}\frac{1}{j+1}(1 - e^{-(j+1)\frac{E_{th}}{\Lambda}}), & 1 < i < M, \\ e^{-M\frac{E_{th}}{\Lambda}} & i = M, \end{cases} \tag{4.9}$$

4.3.3 Throughput Performance Analysis for the MISO System

We are interested in the average throughput of the MISO system, which can be calculated as

$$R = \sum_{i=1}^{M} \Pr[M_a = i]R_i, \tag{4.10}$$

where $\Pr[M_a = i]$ denotes the probability that i beams are usable, given in (4.9), R_i is the average throughput when i beams are usable, which can be calculated using the distribution of the largest SNR among all usable beams, as

$$R_i = \int_0^\infty \log_2(1+x) f_{\gamma_{1:M_a}}(x) dx, \quad i = 1, 2, \ldots, M, \tag{4.11}$$

where $f_{\gamma_{1:M_a}}(x)$ is the PDF of the largest received SNR $\gamma_{1:M_a}$ at the user, given by [29]

$$f_{\gamma_{1:M_a}}(x) = \frac{M_a}{\overline{\gamma}} e^{-\frac{x}{\overline{\gamma}}} (1 - e^{-\frac{x}{\overline{\gamma}}})^{M_a - 1}, \tag{4.12}$$

where $\overline{\gamma}$ denotes the common average received SNR for each beam. By sustituting (4.12) into (4.10) and some manipulation, the close form expression of the throughput of the MISO system can be calculated as

$$R = \sum_{i=1}^{M} \Pr[M_a = i] \left\{ \frac{M_a}{\ln 2} \sum_{n=0}^{M_a - 1} (-1)^{n+1} C_{M_a-1}^{n} \frac{e^{\frac{n+1}{\overline{\gamma}_S}}}{n+1} \mathrm{Ei}\left(- \frac{n+1}{\overline{\gamma}} \right) \right\}, \tag{4.13}$$

where $\mathrm{Ei}(\cdot)$ is the exponential integral function.

4.3.4 Energy Harvesting Performance Analysis

To evaluate the energy harvesting performance, we derive the exact statistical distribution of the harvested energy over one coherence time T_c at the sensor, which can be used for calculating average harvested energy, as well as packet transmission performance of the sensor [31]. Conditioning on the number of usable beams for transmission, the cumulative distribution function (CDF) of E_H can be represented as

$$F_{E_H}(x) = \sum_{m=1}^{M} \Pr[E_H < x, M_a = m]. \tag{4.14}$$

According to our proposed cooperative beam selection scheme, the BS selects the best beam from all M_a usable beams to achieve the largest throughput, whereas the probability that each of M_a usable beams is selected to charge the sensor is equal to

$\frac{1}{M_a}$. Therefore, we can rewrite (4.14) as

$$F_{E_H}(x) = \sum_{m=1}^{M-1} \frac{1}{m} \sum_{i=1}^{m} \Pr\left[E_{i:M} < x, E_{m:M} \geq E_{th}, E_{m+1:M} < E_{th}\right] + \Pr[E_{1:M} < x, E_{1:M} < E_{th}] + \frac{1}{M} \sum_{i=1}^{M} \Pr\left[E_{i:M} < x, E_{M:M} \geq E_{th}\right]. \quad (4.15)$$

For the case of $x \leq E_{th}$, (4.15) can be simply calculated as

$$F_{E_H}(x) = \Pr[E_{1:M} < x] = \int_0^{\frac{x}{\Lambda}} f_{\alpha_{1:M}}(y)dy, \quad x \leq E_{th}, \quad (4.16)$$

By substituting (4.6) into (4.16), $F_{E_H}(x)$ can be calculated as

$$F_{E_H}(x) = M \sum_{j=0}^{M-1} \binom{M-1}{j} \frac{(-1)^j}{j+1} (1 - e^{-(j+1)\frac{x}{\Lambda}}), \; x \leq E_{th}. \quad (4.17)$$

For the case of $x > E_{th}$, (4.26) can be rewritten as

$$\begin{aligned} F_{E_H}(x) \;=\; & \sum_{m=1}^{M-1} \frac{1}{m} \Bigg\{ \int_{\frac{E_{th}}{\Lambda}}^{\frac{x}{\Lambda}} \int_0^{\frac{E_{th}}{\Lambda}} f_{\alpha_{m:M},\alpha_{m+1:M}}(y,z)dydz \\ & + \sum_{i=1}^{m-1} \int_{\frac{E_{th}}{\Lambda}}^{\frac{x}{\Lambda}} \int_{\frac{E_{th}}{\Lambda}}^{w} \int_0^{\frac{E_{th}}{\Lambda}} f_{\alpha_{i:M},\alpha_{m:M},\alpha_{m+1:M},}(w,y,z)dwdydz \Bigg\} \\ & + \frac{1}{M} \Bigg\{ \int_{\frac{E_{th}}{\Lambda}}^{\frac{x}{\Lambda}} f_{\alpha_{M:M}}(y)dy + \sum_{i=1}^{M-1} \int_{\frac{E_{th}}{\Lambda}}^{\frac{x}{\Lambda}} \int_{\frac{E_{th}}{\Lambda}}^{y} f_{\alpha_{i:M},\alpha_{M:M},}(y,z)dydz \Bigg\} \\ & + \int_0^{\frac{E_{th}}{\Lambda}} f_{\alpha_{1:M}}(y)dy, \quad x > E_{th}, \end{aligned} \quad (4.18)$$

where the joint PDF of $\alpha_{i:M}$, $\alpha_{m:M}$ and $\alpha_{m+1:M}$, and the joint PDF of $\alpha_{i:M}$ and $\alpha_{M:M}$ can be given by

$$f_{\alpha_{i:M},\alpha_{m:M},\alpha_{m+1:M}}(x,y,z) \;= \frac{M!e^{-ix-y-z}(e^{-y}-e^{-x})^{m-i-1}(1-e^{-z})^{M-m-1}}{(i-1)!(m-i-1)!(M-m-1)!}, x > y > z, \quad (4.19)$$

$$f_{\alpha_{i:M},\alpha_{M:M}}(y,z) = \frac{M!}{(i-1)!(M-i-1)!} e^{-iy-z}(e^{-z}-e^{-y})^{M-i-1}, \quad y > z, \quad (4.20)$$

respectively[29]. By substituting (4.6), (4.7), (4.19) and (4.20) into (4.18) and carrying out integrations, we can obtain the closed form expression of $F_{E_H}(x)$ for $x > E_{th}$ as

$$
\begin{aligned}
F_{E_H}(x) = &\sum_{m=1}^{M-1} \frac{1}{m} \Bigg\{ \sum_{j=0}^{M-m-1} \binom{M-m-1}{j} \frac{(-1)^j}{j+1} (1 - e^{-(j+1)\frac{E_{th}}{\Lambda}}) \Bigg\} \times \Bigg\{ \frac{M!(e^{-m\frac{E_{th}}{\Lambda}} - e^{-m\frac{x}{\Lambda}})}{m!(M-m-1)!} \\
&+ \sum_{i=1}^{m-1} \frac{M!}{(i-1)!(m-i-1)!(M-m-1)!} \sum_{k=0}^{m-i-1} \binom{m-i-1}{k} \frac{(-1)^{m-i-k-1}}{k+1} \\
&\times \left[e^{-(k+1)\frac{E_{th}}{\Lambda}} \frac{e^{-(m-k-1)\frac{E_{th}}{\Lambda}} - e^{-(m-k-1)\frac{x}{\Lambda}}}{m-k-1} - \frac{e^{-m\frac{E_{th}}{\Lambda}} - e^{-m\frac{x}{\Lambda}}}{m} \right] \Bigg\} + \frac{1}{M} \Bigg\{ e^{-M\frac{E_{th}}{\Lambda}} - e^{-M\frac{x}{\Lambda}} \\
&+ \sum_{i=1}^{M-1} \frac{M!}{(i-1)!(M-i-1)!} \sum_{j=0}^{M-i-1} \binom{M-i-1}{j} \frac{(-1)^{M-i-j-1}}{j+1} \\
&\left[\frac{e^{-(j+1)\frac{E_{th}}{\Lambda}}}{M-j-1} (e^{-(M-j-1)\frac{E_{th}}{\Lambda}} - e^{-(M-j-1)\frac{x}{\Lambda}}) - \frac{1}{M} (e^{-M\frac{E_{th}}{\Lambda}} - e^{-M\frac{x}{\Lambda}}) \right] \Bigg\} \\
&+ M \sum_{j=0}^{M-1} \binom{M-1}{j} \frac{(-1)^j}{j+1} (1 - e^{-(j+1)\frac{E_{th}}{\Lambda}}), \qquad x \geq E_{th}. \qquad (4.21)
\end{aligned}
$$

After taking derivative of (4.29) and (4.21), the closed-form expression of the PDF of the harvested energy over one coherence time can be calculated as

$$
\begin{aligned}
f_{E_H}(x) \;=\; &\\
&\begin{cases}
\frac{M}{\Lambda} \sum_{j=0}^{M-1} (-1)^j \binom{M-1}{j} e^{-(j+1)\frac{x}{\Lambda}}, & x < E_{th}, \\
\sum_{m=1}^{M-1} \frac{e^{-m\frac{x}{\Lambda}}}{m\Lambda} \Bigg\{ \sum_{j=0}^{M-m-1} \binom{M-m-1}{j} \frac{(-1)^j}{j+1} (1 - e^{-(j+1)\frac{E_{th}}{\Lambda}}) \Bigg\} & \\
\times \Bigg\{ \frac{M!}{(m-1)!(M-m-1)!} + \sum_{i=1}^{m-1} \frac{M!}{(i-1)!(m-i-1)!(M-m-1)!} & \\
\sum_{k=0}^{m-i-1} \binom{m-i-1}{k} \frac{(-1)^{m-i-k-1}}{k+1} \left[e^{-\frac{(k+1)(E_{th}-x)}{\Lambda}} - 1 \right] \Bigg\} & \qquad (4.22) \\
+ \frac{e^{-M\frac{x}{\Lambda}}}{M\Lambda} \Bigg\{ M + \sum_{i=1}^{M-1} \frac{M!}{(i-1)!(M-i-1)!} \sum_{k=0}^{M-i-1} \binom{M-i-1}{k} \frac{(-1)^{M-i-k-1}}{k+1} & \\
\left[e^{-\frac{(k+1)(E_{th}-x)}{\Lambda}} - 1 \right] \Bigg\}, & x \geq E_{th},
\end{cases}
\end{aligned}
$$

which can be used to calculate the average harvested energy $\overline{E}_H$ in closed-form as

$$\begin{aligned}
\overline{E}_H &= \int_0^\infty x f_{E_H}(x)dx \\
&= M\sum_{j=0}^{M-1}(-1)^j\binom{M-1}{j}\left[\frac{-E_{th}}{j+1}e^{-(j+1)\frac{E_{th}}{\Lambda}}+\frac{\Lambda}{(j+1)^2}(1-e^{-(j+1)\frac{E_{th}}{\Lambda}})\right] \\
&\quad+\sum_{m=1}^{M-1}\frac{e^{-m\frac{E_{th}}{\Lambda}}}{m}\left\{\sum_{j=0}^{M-m-1}\binom{M-m-1}{j}\frac{(-1)^j}{j+1}(1-e^{-(j+1)\frac{E_{th}}{\Lambda}})\right\}\times \\
&\quad\left\{\frac{M!(E_{th}+\frac{\Lambda}{m})}{m!(M-m-1)!}+\sum_{i=1}^{m-1}\frac{M!}{(i-1)!(m-i-1)!(M-m-1)!}\right. \\
&\quad\left.\sum_{k=0}^{m-i-1}\binom{m-i-1}{k}\frac{(-1)^{m-i-k-1}}{k+1}\left[\frac{E_{th}}{m-k-1}+\frac{\Lambda}{(m-k-1)^2}-\frac{E_{th}}{m}-\frac{\Lambda}{m^2}\right]\right\} \\
&\quad+\frac{e^{-M\frac{E_{th}}{\Lambda}}}{M}\left\{E_{th}+\frac{\Lambda}{M}+\sum_{i=1}^{M-1}\frac{M!}{(i-1)!(M-i-1)!}\sum_{k=0}^{M-i-1}\binom{M-i-1}{k}\frac{(-1)^{M-i-k-1}}{k+1}\right. \\
&\quad\left.\left[\frac{E_{th}}{M-k-1}+\frac{\Lambda}{(M-k-1)^2}-\frac{E_{th}}{M}-\frac{\Lambda}{M^2}\right]\right\}. \qquad (4.23)
\end{aligned}$$

In Fig. 4.2, we plot the PDF of the harvested energy with $E_{th} = 0.0006J$ and $M = 4$ antennas in comparison with the simulation results. As we can see, the analytical result matches the simulation result perfectly, where the harvested energy concentrates around the energy threshold E_{th}, as expected.

4.3.5 Numerical Examples

In Fig. 4.3, we plot the average harvested energy $\overline{E}_H$ as a function of the energy threshold E_{th} for different antenna number M. We can observe that more antennas leads to larger average harvested energy, as expected. We can also see that the average harvested energy at the sensor quickly increases as E_{th} increased, and gradually converges to a constant value when E_{th} is large. This is because when E_{th} is large enough, the BS will only use the best beam to charge the sensor.

In Fig. 4.4, we plot the average throughput of the MISO system as a function of the energy threshold E_{th} for different antenna number M. We can observe that larger antenna number leads to larger throughput, due to the beam selection benefit. We also observe that the throughput reduces gradually to a constant value with the increase of E_{th}. This is because when E_{th} is large, the BS will only use the best beam, from the energy harvesting perspective, to serve its selected user. Combined

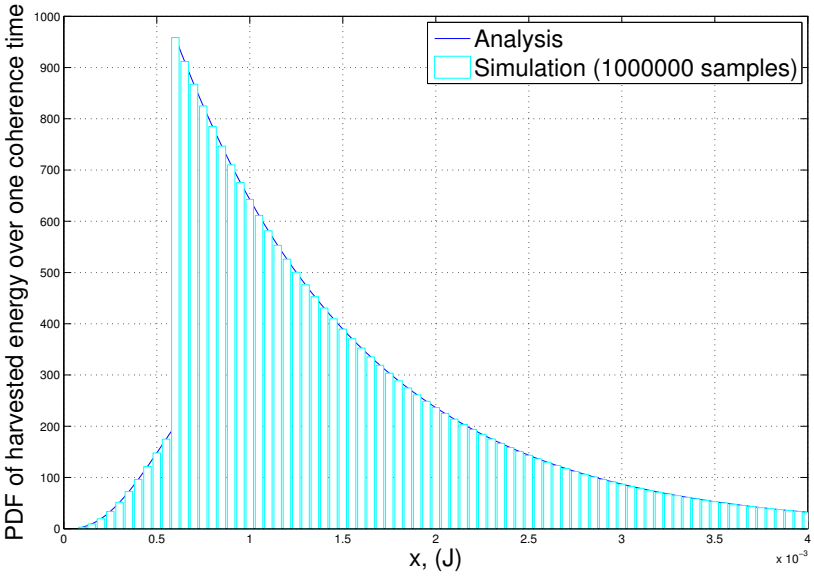

Figure 4.2: Distribution of harvested energy at the sensor.

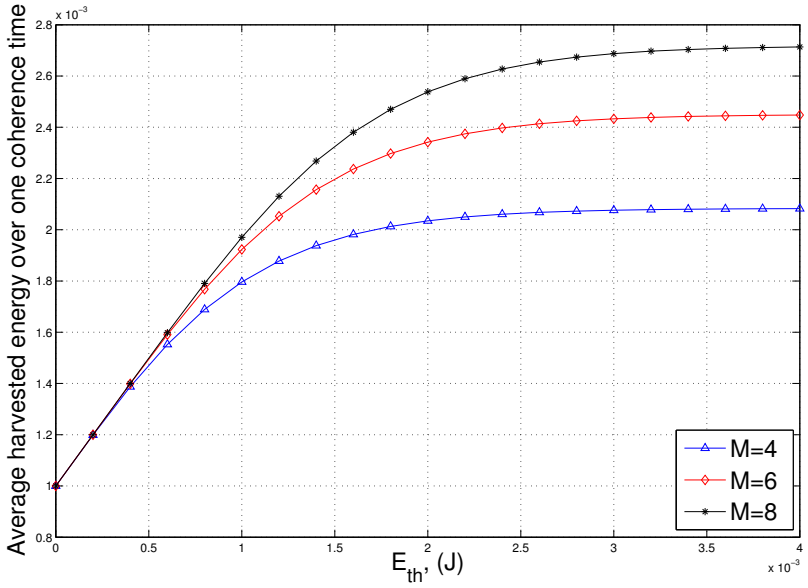

Figure 4.3: Average harvested energy at the sensor.

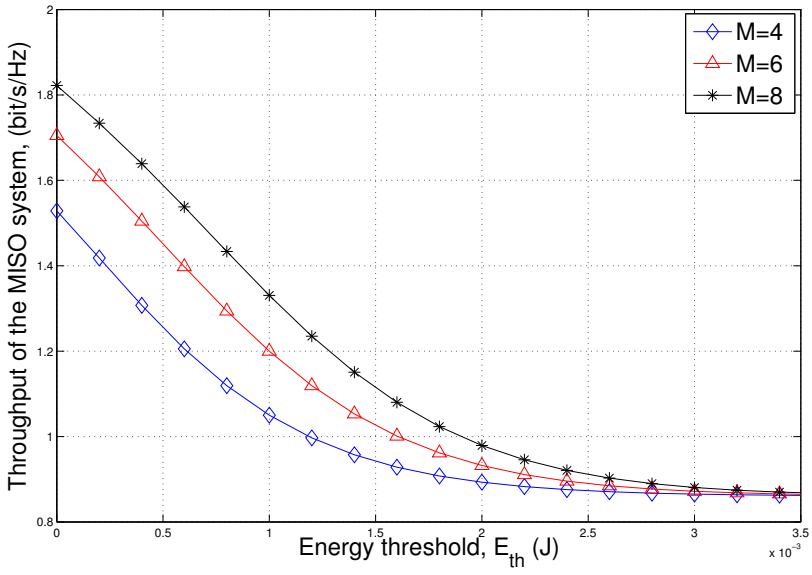

Figure 4.4: Throughput of the MISO system.

with Fig. 4.3, we can see there exists a tradeoff of average harvested energy at the sensor versus throughput of the MISO system. In particular, larger E_{th} leads to larger average harvested energy, but smaller throughput. We can achieve desired energy harvesting performance by properly adjusting E_{th} at the expense of certain throughput degradation in the MISO system.

4.4 RUB-based Cooperative Energy Harvesting for Multiple Sensors

4.4.1 Mode of Cooperation

With the proposed cooperative energy harvesting scheme, the BS will select a maximal number of active beams to serve its users, while ensuring that the harvested energy at the sensor node during each coherence time is above E_{th}.

At the beginning of each channel coherence time, the BS first estimates the channel vector from the BS to the sensor. The BS then calculates and ranks the projection amplitude square α_m for each beam, the order version of which is denoted by $\alpha_{m:M}$, where $\alpha_{1:M} \geq \alpha_{2:M} \geq \cdots \geq \alpha_{M:M}$. After that, the BS calculates the total amount of RF energy that the sensor can harvest when the BS uses m best beams, corresponding to $\alpha_{1:M}$ to $\alpha_{m:M}$. The total harvested energy, dented by E_H, can be given by $E_H = \sum_{i=1}^{m} E_{i,m}$, where $E_{i,m}$ denotes the harvested energy from the ith best beam with projection amplitude square $\alpha_{i:M}$, when m best beams are used for transmission, given by

$$E_{i,m} = \left(\frac{\eta T_c}{\Gamma d_H^{\lambda}}\right)\left(\frac{P_T}{m}\right)\alpha_{i:M}, \quad i = 1, 2, \ldots, m. \tag{4.24}$$

If the harvested energy with m best beams is larger than the predefined energy threshold E_{th}, whereas the harvested energy with $m+1$ best beams is less than E_{th}, i.e. $\sum_{i=1}^{m} E_{i,m} \geq E_{th}$, and $\sum_{i=1}^{m+1} E_{i,m+1} < E_{th}$, then the BS uses the m best beams to serve its users. Note that with constant total transmission power used at the BS and uniform power allocation, the sensor can harvest more energy from less active beams, because the transmission power concentrates on the better beams, i.e. with larger projection power.

4.4.2 Energy Harvesting Performance Analysis

Conditioning on the number of active beams for transmission, denoted by M_a, the cumulative distribution function (CDF) of E_H can be represented as

$$F_{E_H}(x) = \sum_{m=1}^{M} \Pr[E_H < x, M_a = m]. \tag{4.25}$$

According to our proposed cooperative beam selection scheme, the number of active beams M_a is equal to m $(1 < m < M)$ if and only if $\sum_{i=1}^{m} E_{i,m} \geq E_{th}$, and $\sum_{i=1}^{m+1} E_{i,m+1} < E_{th}$. Furthermore, the number of active beams M_a is equal to 1 if the energy threshold E_{th} can not be satisfied with all transmission power P_T allocated to the best beam, i.e., $E_{1,1} < E_{th}$, and equal to M if the harvested energy is larger than E_{th} with P_T allocated to all M beams, i.e., $\sum_{i=1}^{M} E_{i,M} \geq E_{th}$. Therefore, we can rewrite (4.25) as

$$\begin{aligned} F_{E_H}(x) &= \sum_{m=1}^{M-1} \Pr\left[\sum_{i=1}^{m} E_{i,m} < x, \sum_{i=1}^{m} E_{i,m} \geq E_{th}, \sum_{i=1}^{m+1} E_{i,m+1} < E_{th}\right] \\ &\quad + \Pr[E_{1,1} < x, E_{1,1} < E_{th}] + \Pr\left[\sum_{i=1}^{M} E_{i,M} < x, \sum_{i=1}^{M} E_{i,M} \geq E_{th}\right]. \end{aligned} \tag{4.26}$$

For notational conciseness, we denote the sum of the m largest projection amplitude square from $\alpha_{1:M}$ to $\alpha_{m:M}$ as z_m, i.e. $z_m = \sum_{i=1}^{m} \alpha_{i:M}$. It follows that $\sum_{i=1}^{m} E_{i,m} = \left(\frac{\eta T_c}{\Gamma d_H^{\lambda}}\right)\left(\frac{P_T}{m}\right) z_m$. For the case of $x \leq E_{th}$, (4.26) can be simply calculated as

$$F_{E_H}(x) = \Pr[E_{1,1} < x] = \int_0^{\frac{\mu x}{E_{th}}} f_{z_1}(y)dy, \quad x \leq E_{th}, \tag{4.27}$$

where $f_{z_1}(x)$ denotes the PDF of z_1, given by [14, eq. (3.1)]

$$f_{z_1}(x) = Me^{-x}(1 - e^{-x})^{M-1}, \tag{4.28}$$

μ is a constant value equal to $\frac{E_{th}\Gamma d_H^{\lambda}}{\eta T_c P_T}$ for notational conciseness. By substituting (4.28) into (4.27), $F_{E_H}(x)$ can be calculated as

$$F_{E_H}(x) = \frac{\mu M}{E_{th}} e^{-\frac{\mu x}{E_{th}}} (1 - e^{-\frac{\mu x}{E_{th}}})^{M-1}, \quad x \leq E_{th}. \tag{4.29}$$

For the case of $x > E_{th}$, (4.26) can be mathematically calculated, while noting $\Pr[E_{1,1} < x, E_{1,1} < E_{th}]$ is equal to 0, as

$$F_{E_H}(x) = \sum_{m=1}^{M-1} \left\{ \int_0^{\mu} \int_{m\mu}^{(m+1)\mu-y} f_{\alpha_{m+1:M},z_m}(y,z)dydz \right. \tag{4.30}$$
$$\left. - \int_0^{(m+1)\mu-\frac{m\mu x}{E_{th}}} \int_{\frac{m\mu x}{E_{th}}}^{(m+1)\mu-y} f_{\alpha_{m+1:M},z_m}(y,z)dydz \right\} + \int_{M\mu}^{\frac{M\mu x}{E_{th}}} f_{z_M}(y)dy, \quad x > E_{th},$$

where $f_{z_M}(x)$ and $f_{\alpha_{m+1},z_m}(x)$ denote the PDF of z_M, and the joint PDF of α_{m+1} and z_m, respectively, the closed-form expression of which can be obtained as [14, eq. (3.19) and (3.31)]

$$f_{z_M}(x) = \frac{x^{M-1}e^{-x}}{(M-1)!}, \tag{4.31}$$

and

$$f_{\alpha_{m+1:M},z_m}(x,y) = \sum_{i=0}^{M-m-1} \frac{(-1)^i M!(y-mx)^{m-1}e^{-y-(i+1)x}}{(M-m-1-i)!m!(m-1)!i!}, \quad y \geq mx, \tag{4.32}$$

respectively. By substituting (4.31) and (4.32) into (4.30) and carrying out integrations, we can obtain the closed form expression of $F_{E_H}(x)$ for $x > E_{th}$ [36]. After taking derivative of (4.29) and (4.30), the closed-form expression of the PDF of the

harvested energy over one coherence time can be calculated as

$$
\begin{aligned}
f_{E_H}(x) \;=\; & \\
\Bigg\{ & \Bigg\{ \sum_{m=1}^{M-1} \Bigg\{ \sum_{i=1}^{M-m-1} \tfrac{(-1)^{i+1} M!}{(M-m-1-i)!m!(m-1)!i!} \sum_{j=0}^{m-1} \tbinom{m-1}{j} (-m)^{m-1-j} \sum_{t=0}^{j} \tfrac{j!}{(j-t)!} \\
& \Bigg\{ \tfrac{(m-1-j)!}{(i+1)^{m-j}} \left(\tfrac{m\mu}{E_{th}}\right)^{j-t} e^{-\frac{m\mu x}{E_{th}}} x^{j-t-1} \left(j-t-\tfrac{m\mu x}{E_{th}}\right) - \left(\tfrac{m\mu}{E_{th}}\right)^{j-t} e^{-(i+1)(m+1)\mu} \\
& \sum_{r=0}^{m-j-1} \tfrac{(m-1-j)!}{(m-1-j-r)!(i+1)^{r+1}} \sum_{u=0}^{m-1-j-r} (-1)^u \tbinom{m-1-j-r}{u} \left(\tfrac{m\mu}{E_{th}}\right)^{u} [(m+1)\mu]^{m-1-j-r-u} \\
& e^{im\mu\frac{x}{E_{th}}} x^{j-t+u-1} \left(j-t+u+\tfrac{im\mu x}{E_{th}}\right) + e^{-(i+1)(m+1)\mu} \sum_{s=0}^{j-t} \tbinom{j-t}{s} (-1)^s \big[(m+1)\mu\big]^{j-t-s} \\
& \sum_{r=0}^{m-1-j+s} \tfrac{(m-1-j+s)!}{(m-1-j+s-r)!i^{r+1}} \sum_{u=0}^{m-1-j+s-r} (-1)^u \tbinom{m-1-j+s-r}{u} \\
& \left(\tfrac{m\mu}{E_{th}}\right)^{u} [(m+1)\mu]^{m-1-j+s-r-u} x^{u-1} e^{im\mu\frac{x}{E_{th}}} \left(u+\tfrac{im\mu}{E_{th}}x\right) \Bigg\} - \tfrac{M!}{(M-m-1)!m!(m-1)!} \\
& \sum_{j=0}^{m-1} \tbinom{m-1}{j} (-m)^{m-1-j} \sum_{t=0}^{j} \tfrac{j!}{(j-t)!} \Bigg\{ e^{-(m+1)\mu} \sum_{s=0}^{j-t} \tbinom{j-1}{s} (-1)^s \tfrac{m\mu}{E_{th}} \big[(m+1)\mu\big]^{j-t-s} \\
& \left[(m+1)\mu - \tfrac{m\mu x}{E_{th}}\right]^{m-1-j+s} + (m-1-j)! \left(\tfrac{m\mu}{E_{th}}\right)^{j-t} e^{-m\mu\frac{x}{E_{th}}} x^{j-t-1} \left(j-t-\tfrac{m\mu}{E_{th}}x\right) \\
& - \left(\tfrac{m\mu}{E_{th}}\right)^{j-t} e^{-(m+1)\mu} \sum_{r=0}^{m-j-1} \tfrac{(m-1-j)!}{(m-1-j-r)!} \sum_{u=0}^{m-1-j-r} (-1)^u \tbinom{m-1-j-r}{u} \\
& \left(\tfrac{m\mu}{E_{th}}\right)^{u} [(m+1)\mu]^{m-1-j-r-u} (j-t+u) x^{j-t+u-1} \Bigg\} \Bigg\} \mathcal{U}\left(\left(1+\tfrac{1}{m}\right)E_{th} - x\right) \\
& + \sum_{s=0}^{M-1} \Bigg\{ -(M-1-s) + \tfrac{M\mu x}{E_{th}} \Bigg\} \tfrac{(M\mu)^{M-1-s} x^{M-2-s} e^{-\frac{M\mu x}{E_{th}}}}{(M-1-s)! E_{th}^{M-1-s}} \Bigg\} \mathcal{U}(x - E_{th}) \\
& + \tfrac{\mu M}{E_{th}} e^{-\frac{\mu x}{E_{th}}} \left(1 - e^{-\frac{\mu x}{E_{th}}}\right)^{M-1} \mathcal{U}(E_{th} - x),
\end{aligned}
\tag{4.33}
$$

which can be used to calculate the average harvested energy $\overline{E}_H$ in closed-form [36]. In Fig. 4.5, we plot the PDF of the harvested energy with $E_{th} = 0.006J$ and $M = 4$ antennas in comparison with the simulation results. As we can see, the analytical result matches the simulation result perfectly, where the harvested energy concentrates around the energy threshold E_{th}, as expected.

In Fig. 4.6, we plot the average harvested energy $\overline{E}_H$ as a function of the energy threshold E_{th} for different antenna number M. We can see the average harvested energy at the sensor quickly increases as E_{th} increased, and gradually converges to a constant value when E_{th} is large. This is because when E_{th} is large enough, the BS will only use the best beam to charge the sensor. We also observe that more antennas leads to smaller average harvested energy when E_{th} is small, and larger average harvested energy when E_{th} is large. This is because when E_{th} is small, more

antennas leads to more potential active beams, which leads to wider distribution of BS transmit power. When E_{th} is large, the sensor can enjoy more benefits from best beam selection. When E_{th} is 0, the MIMO system serves its users with all beams, and the amount of energy that the sensor can harvest is the same as [31] without considering energy sensitivity and storage capacity.

In Fig. 4.7, we plot the average sum-rate of the multiuser MIMO system as a function of the energy threshold E_{th} for different user number K with M=4 antennas, assuming the user selection scheme proposed in [35] used to maximize the sum-rate of the multiuser MIMO system. We can observe that larger user number leads to larger sum-rate, due to user selection. We also observe that the sum-rate reduces gradually to a constant value with the increase of E_{th}. This is because when E_{th} is large, the BS will only use the best beam, from the energy harvesting perspective, to serve its selected user. Especially, while the sum-rate for the case with $K = 100$ users remains larger than the sum-rate for the case with $K = 50$ users for any value of E_{th}, the sum-rate difference gradually converges to a constant value when E_{th} goes to infinity. Combined with Fig. 4.6, we can see there exists a tradeoff of average harvested energy at the sensor versus sum-rate of the multiuser MIMO system. In particular, larger E_{th} leads to larger average harvested energy, but smaller sum-rate. We can achieve desired energy harvesting performance by properly adjusting E_{th} at the expense of certain sum-rate degradation in the multiuser MIMO system.

4.5 Concluding Remarks

We proposed a RUB-based cooperative beam selection scheme, using which the existing multiuser MIMO system can help increase the amount of harvested energy of wireless sensor nodes. We considered both single user case and multiuser case for the existing MIMO system. We obtained the closed-form expression of the distribution of harvested energy and the average harvested energy of the sensor node, based on which, we investigate the tradeoff of the average harvested energy versus the sum-rate of the multiuser MIMO system.

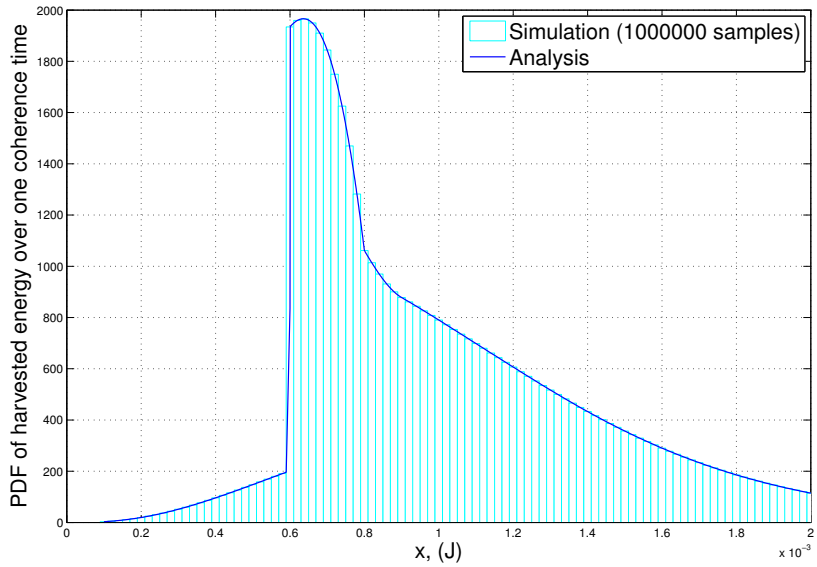

Figure 4.5: Distribution of harvested energy at the sensor.

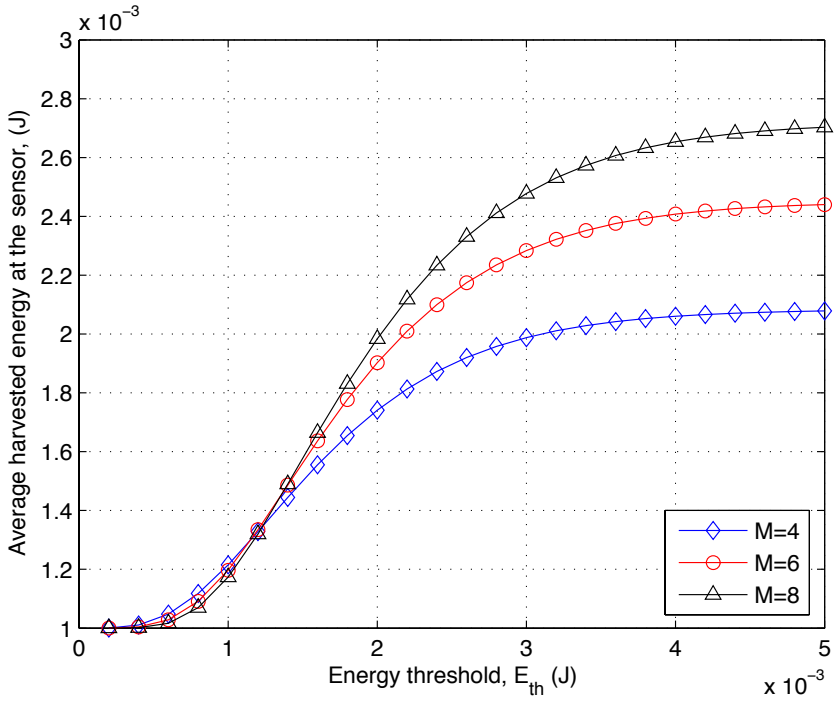

Figure 4.6: Average harvested energy at the sensor.

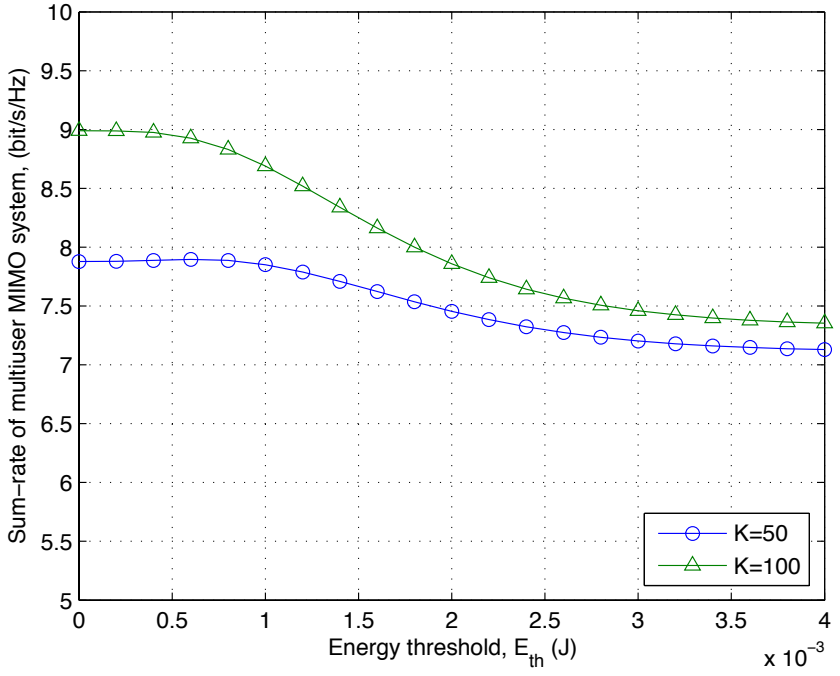

Figure 4.7: Sum-rate of multiuser MIMO system for M=4 antennas.

Chapter 5

Conclusion and Future Work

This dissertation focussed mainly on the low complexity cooperation solutions for RF energy harvesting from existing wireless communication systems. First of all, we considered an underlay cognitive radio, which is a potential candidate technology of the next generation wireless communication systems. Particularly, we considered two low complexity cooperation schemes to ensure the performance requirement of the primary system, while the multi-user MIMO secondary system also selects the best beam to serve its users. We then introduced some theoretical results regarding RF-energy-powered sensor transmission. Specifically, we presented the exact distribution of harvested energy over a certain number channel coherence time with the consideration of hardware limitation, such as energy harvesting sensitivity and harvesting efficiency. We also analyzed the delay and packet loss performance of sensor transmission and proposed the optimal design of energy storage capacity of the sensor nodes to minimize the average packet transmission delay with two candidate transmission strategies for delay insensitive traffics. In the last part of this dissertation, we proposed low complexity cooperative beam selection schemes between RF-energy-powered wireless sensor node and existing multi-user multi-antenna system. We analyzed the performance of both RF energy harvesting for the sensor node and sum-rate for the existing system.

We believe that this work can be extended further in many directions in the future. For example, we can extend the analysis from Rayleigh fading channel to other fading channel environment to quantify the performance of RF energy harvesting for wireless sensor networks. We can also use the asymptotic analysis, which examine the performance of the overlaid sensor transmission when certain system parameters, e.g. transmission power, number of antennas, etc, approaches infinity. Furthermore, the

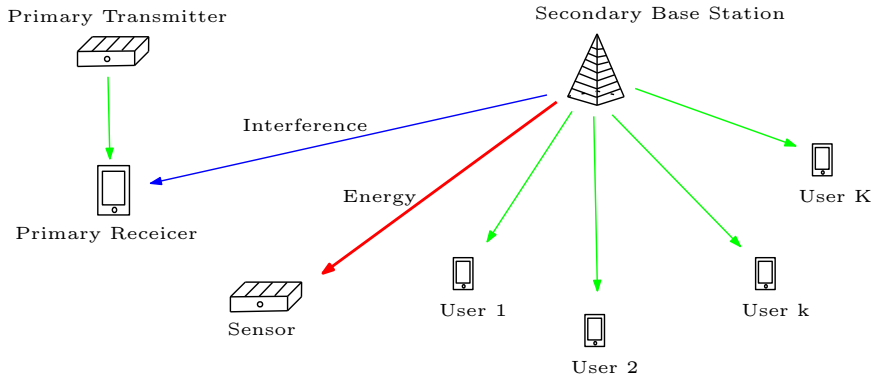

Figure 5.1: Three-system model.

proposed cooperative RF energy harvesting schemes are designed just for single sensor transmission. These schemes can be extended to a multiple-sensor wireless sensor networks after proper adjustments. For example, we can investigate the maximal number of RF-energy-powered-sensors that can be deployed in the coverage of existing multi-user MIMO system while the requirement of both systems are satisfied. Lastly, the analysis of these schemes would not only help the researcher to analyze and predict their performance for a target application but will also pave the way to modify these schemes to achieve better performance with minimal increase in the computational complexity.

Specifically, we consider a three-system model shown in Fig. 5.1. A RF-energy-powered-sensor is deployed in the coverage area of existing cognitive systems, where the secondary system is a multiuser MIMO system. The sensor can harvest RF energy from the transmitted signal of the secondary system, and use it as its sole energy source for transmission. The sensor needs to harvest RF energy above a predefined energy threshold from the secondary base station over each channel coherence time, whereas the secondary system should limit its interference to primary receiver below an interference threshold.

We can explore the optimal beamforming design by maximizing the sum-rate of the secondary system, subject to both the energy harvesting and interference constraints for the other two systems. We can also propose low complexity cooperative strategies to satisfy the requirement of each system simultatenously. We assume that the secondary system uses RUB transmission, which requires very low feedback. We can propose *priority-based two-round beam selection schemes, depending on whether the primary receiver or the sensor has the first priority.* For example, when the sensor

has the first priority, the secondary system will select a beam vector β_{1st} that can satisfy the energy requirement for the first beam selection round. Then for the second round, the secondary system will further select beams from β_{1st} to limit interference to primary receiver below the interference threshold. After that, the secondary system allocates all available beams to serve its SUs. Then we can analyze and compare the performance of the two schemes, together with the beamforming design optimization results. We may also consider single SU case for the secondary system as a separate work.

List of Publications

[1] T.-Q Wu and H.-C Yang, "Performance analysis for RUB-based cognitive radio network with cooperative beam selection," *80th IEEE Vehicular Technology Conference*, pp. 1-5, 2014.

[2] T.-Q Wu and H.-C Yang, "RF energy harvesting with cooperative beam selection for wireless sensors," *IEEE Wireless Communications Letters*, vol. 3, no. 6, pp. 585-588, Dec. 2014.

[3] T.-Q Wu and H.-C Yang, "Packet loss rate analysis of wireless sensor transmission with RF energy harvesting," *CrownCom 2015*, pp. 620-630, April 2015.

[4] T.-Q Wu and H.-C Yang, "On the performance of overlaid wireless sensor transmission with RF energy harvesting," *IEEE Journal on Selected Areas in Communications*, vol. 33, no. 8, pp. 1693-1705, Aug. 2015.

[5] W. Li, T.-Q Wu and H.-C Yang, "Enhancing RF energy harvesting performance with cooperative beam selection for wireless sensors," *IEEE Pacific Rim Conference on Communications, Computers and Signal Processing (PACRIM)*, pp. 524-528, 2015.

[6] T.-Q Wu, H.-C Yang and Y.-C Liang, "Cooperative secondary beam selection for cognitive multiuser MIMO transmission with random beamforming," *IEEE Trans. Cognitive Commu. and Networking*, vol. 2, no. 2, pp. 141-149, June 2016.

References

[1] I. Akyildiz, W. Su, Y. Sankarasubramaniam, and E. Cayirci, "A survey on sensor networks," *Communications Magazine, IEEE,* vol. 40, no. 8, pp. 102-114, Aug. 2002.

[2] W. Seah, Z. A. Eu, and H.-P. Tan, "Wireless sensor networks powered by ambient energy harvesting (wsn-heap) - survey and challenges," in *Wireless Communication, Vehicular Technology, Information Theory and Aerospace Electronic Systems Technology, 2009. Wireless VITAE 2009. 1st International Conference*, pp. 1-5, May 2009.

[3] S. Sudevalayam and P. Kulkarni, "Energy harvesting sensor nodes: survey and implications," *Communications Surveys Tutorials, IEEE,* vol. 13, no. 3, pp. 443-461, 2011.

[4] C. Alippi and C. Galperti, "An adaptive system for optimal solar energy harvesting in wireless sensor network nodes," *IEEE Trans. on Circuits and Systems*, vol. 55, no. 6, pp. 1742-1750, July 2008.

[5] M. Weimer, T. Paing, and R. Zane, "Remote area wind energy harvesting for low-power autonomous sensors," in *37th IEEE Power Electronics Specialists Conference*, pp. 1-5, June 2006.

[6] L. Mateu, C. Codrea, N. Lucas, M. Pollak, and P. Spies, "Energy harvesting for wireless communication systems using thermogenerators," in *Proc. of the XXI Conference on Design of Circuits and Integrated Systems (DCIS)*, Barcelona, Spain, Nov. 2006.

[7] Y. K. Tan, K. Y. Hoe, and S. K. Panda, "Energy harvesting using piezoelectric igniter for self-powered radio frequency (RF) wireless sensors," in *Proc. of IEEE Intl Conference on Industrial Technology (ICIT)*, pp. 1711-1716, Dec. 2006.

[8] T. Le, K. Mayaram, and T. Fiez, "Efficient far-field radio frequency energy harvesting for passively powered sensor networks," *Solid-State Circuits, IEEE Journal of*, vol. 43, no. 5, pp. 1287-1302, May 2008.

[9] V. Liu, A. Parks, V. Talla, S. Gollakota, D. Wetherall, and J. R. Smith, "Ambient backscatter: wireless communication out of thin air," in *Proc. ACM SIGCOMM*, pp. 1-13, Aug. 2013.

[10] U. Baroudi, A. Qureshi, V. Talla, S. Gollakota, S. Mekid, and A. Bouhraoua, "Radio frequency energy harvesting characterization: an experimental study," in *Proc. IEEE TSPCC*, pp. 1976-1981, Feb. 2012.

[11] Powercast Corporation, "TX91501 users manual and P2110s datasheet," http://www.powercastco.com.

[12] J. Yang and S. Ulukus, "Optimal packet scheduling in an energy harvesting communication system," *IEEE Trans. Commu.*, vol. 60, no. 1, pp. 220-230, Jan. 2012.

[13] K. Tutuncuoglu and A. Yener, "Optimum transmission policies for battery limited energy harvesting nodes," *IEEE Trans. Wireless Commu.*, vol. 11, no. 3, pp. 1180-1189, Mar. 2012.

[14] C. Huang, and R. Zhang, and S. Cui, "Throughput maximization for the Gaussian relay channel with energy harvesting constraints," *IEEE J. Sel. Areas Commu.*, vol. 31, no. 8, pp. 1469-1479, Aug. 2013.

[15] O. Ozel, and K. Tutuncuoglu, J. Yang, S. Ulukus, and A. Yener, "Transmission with energy harvesting nodes in fading wireless channels: Optimal policies," *IEEE J. Sel. Areas Commu.*, vol. 29, no. 8, pp. 1732-1743, Sep. 2011.

[16] C. K. Ho and R. Zhang, "Optimal energy allocation for wireless communications with energy harvesting constraints," *IEEE Trans. Signal Process*, vol. 60, no. 9, pp. 4808-4818, Sep. 2012.

[17] J. Yang, O. Ozel, and S. Ulukus, "Broadcasting with an energy harvesting rechargeable transmitter," *IEEE Trans. Wireless Commu.*, vol. 11, no. 2, pp. 571-583, Feb. 2012.

[18] M. Antepli, and E. Uysal-Biyikoglu, and H. Erkal, "Optimal packet scheduling on an energy harvesting broadcast link," *IEEE J. Sel. Areas Commu.*, vol. 29, no. 8, pp. 1721-1731, Sep. 2011.

[19] O. Ozel, J. Yang, and S. Ulukus, "Optimal broadcast scheduling for an energy harvesting rechargeable transmitter with a finite capacity battery," *IEEE Trans. Wireless Commu.*, vol. 11, no. 6, pp. 2193-2203, June 2012.

[20] V. Sharma, U. Mukherji, V. Joesph, and S. Gupta, "Optimal energy management policies for energy harvesting sensor nodes," *IEEE Trans. Wireless Commu.*, vol. 9, no. 4, pp. 1326-1336, Apr. 2010.

[21] F. Iannello, O. Simeone, and U. Spagnolini, "Medium access control protocols for wireless sensor networks with energy harvesting," *IEEE Trans. Commun.*, vol. 60, no. 5, pp. 1381-1389, May 2012.

[22] S. Luo, R. Zhang, and T. J. Lim, "Optimal save-then-transmit protocol for energy harvesting wireless transmitters," *IEEE Trans. Wireless Commu.*, vol. 12, no. 3, pp. 1196-1207, Mar. 2013.

[23] L. R. Varshney, "Transporting information and energy simultaneously," in *Proc. IEEE Int. Symp. Inf. Theory (ISIT)*, pp. 1612-1616, July 2008.

[24] P. Grover and A. Sahai, "Shannon meets Tesla: wireless information and power transfer," in *Proc. IEEE Int. Symp. Inf. Theory (ISIT)*, pp. 2363-2367, June 2010.

[25] R. Zhang and C. K. Ho, "MIMO broadcasting for simultaneous wireless information and power transfer," *IEEE Trans. Wireless Commun.*, vol. 12, no. 5, pp. 1989-2001, May 2013.

[26] S. Park, J. Heo, B. Kim, W. Chung, H. Wang, and D. Hong, "Optimal mode selection for cognitive radio sensor networks with RF energy harvesting," in *Proc. IEEE PIMRC*, pp. 2155-2159, 2012.

[27] L. Liu, R. Zhang, and K. Chua, "Wireless information transfer with opportunistic energy harvesting," *IEEE Trans. Wireless Commun.*, vol. 12, no. 1, pp. 288-300, Jan. 2013.

[28] V. Raghunathan, S. Ganeriwal, and M. Srivastava, "Emerging techniques for long lived wireless sensor networks," *IEEE Commun. Mag.*, vol. 44, no. 4, pp. 108-114, Apr. 2006.

[29] H.-C. Yang and M.-S. Alouini, *Order Statistics in Wireless Communications*. Cambridge University Press, 2011.

[30] A. Goldsmith, *Wireless Communications*. Cambridge University Press, 2005.

[31] T.-Q Wu and H.-C Yang, "On the performance of overlaid wireless sensor transmission with RF energy harvesting," *IEEE Journal on Selected Areas in Communications*, vol. 33, no. 8, pp. 1693-1705, Aug. 2015.

[32] Q. Shi, L. Liu, W. Xu, and R. Zhang, "Joint transmit beamforming and receive power splitting for MISO SWIPT systems," *IEEE Trans. Wireless Commun.*, vol. 13, no. 6, pp. 3269-3280, June 2014.

[33] K. K. J. Chung, C.-S. Hwang, and Y. K. Kim, "A random beamforming technique in MIMO systems exploiting multiuser diversity," *IEEE J. Sel. Areas Commun.*, vol. SAC-21, no. 5, pp. 848-855, June 2003.

[34] M. Sharif and B. Hassibi, "On the capacity of MIMO broadcast channels with partial side information," *IEEE Trans. Inf. Theory*, vol. 51, no. 2, pp. 506-522, Feb. 2005.

[35] H.-C. Yang, P. Lu, H.-K. Sung, and Y.-C. Ko, "Exact sum-rate analysis of MIMO broadcast channel with random unitary beamforming", *IEEE Trans. Commun.*, vol. 59, no. 11, pp. 2982-2986, Nov. 2011.

[36] T.-Q. Wu and H.-C. Yang, "Improved performance of RF energy powered wireless sensor node with cooperative beam selection", Available: arXiv:1405.5507.

[37] T.-Q. Wu and H.-C. Yang, "RF energy harvesting with cooperative beam selection for wireless sensors", accepted by *IEEE Wireless Commun. Letters*.

[38] J. Mitola and J. Maguire,"Cognitive radio: making software radios more personal," *IEEE Personal Commun.*, vol. 6, pp. 13-18, Aug. 1999.

[39] S. Haykin, "Cognitive radio: brain-empowered wireless communications," *IEEE J. Select. Areas Commun.*, vol. 23, no. 2, pp. 201-220, Feb. 2005.

[40] I. F. Akyildiz, W.-Y. Lee, M. C. Vuran, and S. Mohanty, "Next generation/dynamic spectrum access/cognitive radio wireless networks: a survey," *Computer Networks*, vol. 50, no. 13, pp. 2127-2159, 2006.

[41] Y. Xing, C. N. Mathur, M. A. Haleem, R. Chandramouli, and K. P. Subbalakshmi, "Dynamic spectrum access with QoS and interference temperature constraints," *IEEE Trans. Mobile Computing*, vol. 6, no. 4, pp. 423-433, April 2007.

[42] K. Huang and R. Zhang, "Cooperative feedback for multi-antenna cognitive radio networks," *IEEE Trans. Signal Process.*, vol. 59, pp. 747-758, Feb. 2011.

[43] J.-H. Noh and S.-J. Oh, "Beamforming in a multi-user cognitive radio system with partial channel state information," *IEEE Trans. Wireless Communication*, vol.12, no. 2, pp. 616-625, Feb. 2013.

[44] L. Zhang, Y. Liang and Y. Xin, "Joint beamforming and power allocation for multiple access channels in cognitive radio networks," *IEEE J. Selected Areas Commun.*, vol. 26, no. 1, pp. 38-51, Jan. 2008.

[45] G. Zheng, K.-K. Wong, and B. Ottersten, "Robust cognitive beamforming with bounded channel uncertainties," *IEEE Trans. Signal Process.*, vol. 57, pp. 4871-4881, Dec. 2009.

[46] E. Gharavol, Y.-C. Liang, and K. Mouthaan, "Robust downlink beamforming in multiuser MISO cognitive radio networks with imperfect channel-state information," *IEEE Trans. Veh. Technol.*, vol. 59, pp. 2852-2860, July 2010.

[47] J.-H. Noh and S.-J. Oh, "Cognitive radio channel with cooperative multi-antenna secondary systems," *IEEE J. Sel. Areas Commun.*, vol. 32, no. 3, pp. 539-549, Mar. 2014.